Performance of BICM–SC and BICM–OFDM Systems with Diversity Reception in Non–Gaussian Noise and Interference

[1] Amir Nasri and Robert Schober

Department of Electrical and Computer Engineering

The University of British Columbia

2356 Main Mall, Vancouver, BC, V6T 1Z4, Canada

Phone: +604 - 822 - 3515

Fax: +604 - 822 - 5949

E-mail: {amirn, rschober}@ece.ubc.ca

In this paper, we present a general mathematical framework for performance analysis of single–carrier (SC) and orthogonal frequency division multiplexing (OFDM) systems employing popular bit–interleaved coded modulation (BICM) and multiple receive antennas. The proposed analysis is applicable to BICM systems impaired by general types of fading (including Rayleigh, Ricean, Nakagami–m, Nakagami–q, and Weibull fading) and general types of noise and interference with finite moments such as additive white Gaussian noise (AWGN), additive correlated Gaussian noise, Gaussian mixture noise, co–channel interference, narrowband interference, and ultra–wideband interference. We present an approximate upper bound for the bit error rate (BER) and an accurate closed–form approximation for the asymptotic BER at high signal–to–noise ratios for Viterbi decoding with the standard Euclidean distance branch metric. Exploiting the asymptotic BER approximation we show that the diversity gain of BICM systems only depends on the free distance of the code, the type of fading, and the number of receive antennas but not on the type of noise. In contrast their coding gain strongly depends on the noise moments. Our asymptotic analysis shows that as long as the standard Euclidean distance branch metric is used for Viterbi decoding, BICM systems optimized for AWGN are also optimum for any other type of noise and interference with finite moments.

---

[1]This work will be presented in part at the IEEE Global Telecommunications Conference (Globecom), New Orleans, 2008.

1 Introduction

Bit–interleaved coded modulation (BICM) is an efficient technique to extract time diversity in systems with single–carrier (SC) modulation [1] and frequency diversity in systems employing orthogonal frequency division multiplexing (OFDM), and has been adopted by a number of recent standards and is also expected to play a major role in future wireless systems [2].

While wireless systems are usually optimized for additive white Gaussian noise (AWGN), in practice, they are also subject to a multitude of other impairments such as narrowband interference (NBI) [3], co–channel interference (CCI) [4, 5], correlated Gaussian noise and interference [6], man–made impulsive noise [7, 8], and ultra–wideband (UWB) interference [9]–[11]. Therefore, it is of both theoretical and practical interest to investigate how the performance of BICM–SC and BICM–OFDM systems designed for AWGN environments is affected by non–Gaussian noise.[2] We note that almost all existing performance studies of BICM are limited to AWGN. For example, union bounds for the bit error rate (BER) of BICM–SC were provided in [1, 12, 13] and similar expressions for BICM–OFDM can be found in [14]. Sattlepoint approximation techniques for BICM–SC systems were introduced in [15, 16]. The combination of BICM–OFDM and spatial diversity techniques was analyzed in [14, 17, 18]. In contrast, only few analytical results are available for non–AWGN types of noise. Namely, the performance of BICM–SC in Middleton's Class A impulsive noise and of BICM–OFDM in UWB interference was analyzed in [19] and [11], respectively.

Motivated by the lack of general performance results, in this paper, we provide a mathematical framework for performance analysis of BICM–SC and BICM–OFDM systems employing Viterbi decoding with the standard Euclidean distance branch metric [1] and multiple receive antennas in fully interleaved fading and non–AWGN environments. This framework is very general and applicable to arbitrary linear modulation formats, all commonly used fading models, and all practically relevant types of noise with finite moments. We first develop a general approximate upper bound on the BER of BICM systems, which is easy to compute but offers little insight since it requires numerical integration. To overcome this problem, we derive accurate closed–form asymptotic BER approximations for BICM–SC and BICM–OFDM systems which provide significant insight into the impact of system parameters such as the modulation format, the free distance of the code, the type of fading, and

---

[2]In the rest of this paper, the term "noise" refers to any additive impairment of the received signal, and also includes what is commonly referred to as "interference".

the type of noise on performance. In particular, the asymptotic BER expressions reveal that while the diversity gain of BICM systems is not affected by the type of noise, the coding gain depends on certain noise moments. We note that the asymptotic performance of *uncoded* SC modulation has been studied in AWGN [20, 21] and non–AWGN [22, 23] channels before. However, both the analysis techniques and the results in [20]–[23] are not applicable to BICM.

The rest of this paper is organized as follows. In Section 2, the considered BICM–SC and BICM–OFDM system models are introduced. The proposed upper bound and asymptotic approximation for the BER are presented in Sections 3 and 4, respectively. Various practically relevant noise models are discussed in Section 5. The presented analysis is verified via computer simulations in Section 6, and conclusions are drawn in Section 7.

2 System Model

We consider BICM–SC and BICM–OFDM systems with N_R receive antennas. For convenience, in this paper, all signals and systems are represented by their complex baseband equivalents.

2.1 System Model

The BICM transmitter consists of a convolutional encoder of rate R_c, an interleaver, and a memoryless mapper [1]. Specifically, the codeword $\boldsymbol{c} \triangleq [c_1, c_2, \ldots, c_{m_c K_c}]$ of length $m_c K_c$ is generated by a convolutional encoder and interleaved. The interleaved bits are broken up into blocks of m_c bits each, which are subsequently mapped to symbols x_k from a constellation $\mathcal{X}$ of size $|\mathcal{X}| \triangleq M = 2^{m_c}$ to form the transmit sequence $\boldsymbol{x} \triangleq [x_1, x_2, \ldots, x_{K_c}]$ of length K_c. Assuming perfect synchronization and demodulation, for both BICM–SC and BICM–OFDM the signal observed at the N_R receive antennas can be modeled as

$$\boldsymbol{r}_k = \sqrt{\gamma}\,\boldsymbol{h}_k\,x_k + \boldsymbol{n}_k, \qquad 1 \leq k \leq K_c, \tag{1}$$

where $\boldsymbol{h}_k \triangleq [h_{k,1} \ \ldots \ h_{k,N_R}]^T$ with $\mathcal{E}\{||\boldsymbol{h}_k||^2\} = N_R$ and $\boldsymbol{n}_k \triangleq [n_{k,1} \ \ldots \ n_{k,N_R}]^T$ with $\mathcal{E}\{||\boldsymbol{n}_k||^2\} = N_R$ contain the fading gains $h_{k,l}$ and the noise variables $n_{k,l}$, $1 \leq l \leq N_R$, respectively, and γ denotes the signal–to–noise ratio (SNR) per receive antenna.[3] As customary in the literature, cf. e.g. [1, 13,

---

[3]In this paper, $[\cdot]^T$, $(\cdot)^H$, $\Re\{\cdot\}$, $||\cdot||$, $\det(\cdot)$, and $\mathcal{E}_x\{\cdot\}$ denote transposition, Hermitian transposition, the real part of a complex number, the L_2–norm of a vector, the determinant of a matrix, and statistical expectation with

17], for our performance analysis we assume perfect interleaving, which means that $\boldsymbol{h}_k$ and $\boldsymbol{n}_k$ can be modeled as independent, identically distributed (i.i.d.) random vectors and only their first order probability density functions (pdfs) are relevant. Thus, to simplify our notation, in the following, we will drop the time/frequency index k wherever possible. We discuss the assumptions necessary for the validity of the i.i.d. assumption more in detail below.

BICM–SC: For BICM–SC we assume transmission over a flat fading channel and coding over B frames of N data symbols, i.e., $K_c = NB$. The channel is time–variant within one frame and changes independently from frame to frame (e.g. due to frequency hopping). For sufficiently large N and/or B assuming that the time–domain fading vectors $\boldsymbol{h}_k$ are i.i.d. is justified [1].

BICM–OFDM: We consider a BICM–OFDM system with N sub–carriers where one codeword spans B OFDM symbols, i.e., $K_c = BN$. We assume that the length of the OFDM cyclic prefix exceeds the length of the channel impulse response and that the channel changes independently from OFDM symbol to OFDM symbol. Thus, modeling the frequency–domain channel gains $\boldsymbol{h}_k$ as i.i.d. vectors implies that the channel is severely frequency selective and/or B is sufficiently large.

Practical BICM–SC and BICM–OFDM systems that employ interleaving and coding over $B > 1$ frequency–hopped frames include the GSM/EDGE mobile communication system ($N = 116/N = 348$, $B = 8$) and the ECMA multi–band OFDM (MB–OFDM) UWB system ($N = 128$, $B = 3$; future versions of the standard may use up to $B = 15$) [9], respectively.

2.2   Fading and Noise Model

Fading Model: The fading gains can be expressed as $h_l \triangleq a_l e^{j\Theta_l}$, where a_l and Θ_l are mutually independent random variables (RVs). Specifically, Θ_l is uniformly distributed in $[-\pi, \pi)$ and a_l is a positive real RV characterized by its distribution $p_{a,l}(a_l)$ or equivalently by its moment generating function (MGF) $\Phi_{a,l}(s) \triangleq \mathcal{E}\{e^{-sa_l}\}$. Correlated fading can be modeled via the joint pdf $p_{\boldsymbol{a}}(\boldsymbol{a})$ or the joint MGF $\Phi_{\boldsymbol{a}}(\boldsymbol{s}) \triangleq \mathcal{E}\{e^{-\sum_{l=1}^{N_R} s_l a_l}\}$, $\boldsymbol{s} \triangleq [s_1 \ \ldots \ s_{N_R}]^T$, of the elements of $\boldsymbol{a} \triangleq [a_1 \ \ldots \ a_{N_R}]^T$, cf. e.g. [24]–[26]. For the asymptotic analysis in Section 4, we require the fading channel to be

---

respect to x, respectively. Moreover, $\boldsymbol{I}_M$ and $\boldsymbol{0}_M$ are the $M \times M$ identity matrix and the all–zero column vector of length M, respectively. Furthermore, we use the notation $u \stackrel{\circ}{=} v$ to indicate that u and v are asymptotically equivalent, and a function $f(x)$ is $o(g(x))$ if $\lim_{x\to 0} f(x)/g(x) = 0$.

asymptotically spatially i.i.d., i.e., for $\boldsymbol{a} \to \boldsymbol{0}_{N_R}$ the joint pdf can be expressed as

$$p_{\boldsymbol{a}}(\boldsymbol{a}) \doteq \prod_{l=1}^{N_R} p_a(a_l), \tag{2}$$

where

$$p_a(a) = 2\alpha_c a^{2\alpha_d - 1} + o(a^{2\alpha_d - 1}) \tag{3}$$

with fading distribution dependent constants α_c and α_d. Eq. (2) is obvious for i.i.d. and independent, non–identically distributed (i.n.d.) fading [20]–[22], and we prove its validity for the most popular correlated fading models (Rayleigh, Ricean, and Nakagami–m) in Appendix A. For these correlated fading models and for independent Nakagami–q and Weibull fading, the fading pdf $p_{a,l}(a_l)$ and parameters α_c and α_d are specified in Table 1.

Noise Model: The proposed analysis is very general and applicable to all types of noise for which all joint moments of the elements of $\boldsymbol{n}$ exist. This is a mild condition which is met by most practically relevant types of noise and interference, see Section 5 for several examples. An exception is α–stable noise, which is sometimes used to model impulsive noise [27], as the higher order moments of α–stable noise do not exist. Note that our analysis is applicable to other types of impulsive noise such as Middleton's Class–A model and ϵ–mixture noise.

3   Approximate Upper Bound for BER

In this section, we present an approximate upper bound for the BER of BICM systems operating in non–AWGN environments.

3.1   MGF of Metric Difference

We assume Viterbi decoding with the standard Euclidean (ED) branch metric [1]

$$\lambda_i \triangleq \min_{x \in \mathcal{X}_b^i} \left\{ ||\boldsymbol{r} - \sqrt{\gamma}\,\boldsymbol{h}\,x||^2 \right\} \tag{4}$$

for bit i, $1 \le i \le m_c$, of symbol x. Here, $\mathcal{X}_b^i$ denotes the subset of all symbols in constellation $\mathcal{X}$ whose label has value $b \in \{0, 1\}$ in position i. In AWGN, the ED branch metric λ_i performs close to optimum at sufficiently high SNR [1]. In non–Gaussian noise, significant performance gains could be achieved with optimum maximum–likelihood (ML) decoding, which, however, requires knowledge of

the noise pdf. Since this knowledge is typically not available at the receiver, in most practical systems, the ED branch metric is also used in the presence of non–Gaussian impairments. For derivation of the proposed upper bound it is convenient to first calculate the MGF of the metric difference

$$\Delta(x, z) \triangleq ||\boldsymbol{r} - \sqrt{\gamma}\,\boldsymbol{h}\,z||^2 - ||\boldsymbol{r} - \sqrt{\gamma}\,\boldsymbol{h}\,x||^2 = d_{xz}^2\,\gamma||\boldsymbol{h}||^2 - 2\,d_{xz}\sqrt{\gamma}\,\Re\{\boldsymbol{h}^H\boldsymbol{n}\}, \qquad (5)$$

where x denotes the transmitted symbol and z is the nearest neighbor of x in $\mathcal{X}_{\bar{b}}^i$ with $\bar{b}$ being the bit complement of b, and $x - z \triangleq d_{xz}e^{j\Theta_d}$ with ED $d_{xz} > 0$. Since we assume the phases Θ_l of h_l to be uniformly distributed, in (5), we have absorbed $e^{j\Theta_d}$ in $\boldsymbol{h}$ without loss of generality. Based on (5) the MGF $\Phi_{\Delta(x,z)}(s) \triangleq \mathcal{E}_{\boldsymbol{h},\boldsymbol{n}}\{e^{-s\Delta(x,z)}\}$ of $\Delta(x, z)$ can be expressed as

$$\Phi_{\Delta(x,z)}(s) = \mathcal{E}_{\boldsymbol{h}}\{e^{-d_{xz}^2\,\gamma||\boldsymbol{h}||^2\,s}\,\mathcal{E}_{\boldsymbol{n}}\{e^{2\,d_{xz}\sqrt{\gamma}\,\Re\{\boldsymbol{h}^H\boldsymbol{n}\}\,s}\}\} = \mathcal{E}_{\boldsymbol{a}}\{e^{-d_{xz}^2\,\gamma||\boldsymbol{a}||^2\,s}\,\Phi_{\hat{\boldsymbol{n}}}(-2\,d_{xz}\sqrt{\gamma}\,\boldsymbol{a}s)\}, \qquad (6)$$

where $\hat{\boldsymbol{n}} \triangleq [e^{-j\Theta_1}n_1 \ldots e^{-j\Theta_{N_R}}n_{N_R}]^T$ and $\Phi_{\hat{\boldsymbol{n}}}(\boldsymbol{s}) \triangleq \mathcal{E}_{\hat{\boldsymbol{n}}}\{e^{-\boldsymbol{s}^T\,\Re\{\hat{\boldsymbol{n}}\}}\}$ is the MGF of $\hat{\boldsymbol{n}}$. If the phases of the noise components n_l, $1 \le l \le N_R$, are mutually independent and uniformly distributed in $[-\pi, \pi)$, $\Phi_{\hat{\boldsymbol{n}}}(\boldsymbol{s}) = \Phi_{\boldsymbol{n}}(\boldsymbol{s}) \triangleq \mathcal{E}_{\boldsymbol{n}}\{e^{-\boldsymbol{s}^T\,\Re\{\boldsymbol{n}\}}\}$ is valid and $\Phi_{\hat{\boldsymbol{n}}}(\boldsymbol{s})$ in (6) can be replaced by $\Phi_{\boldsymbol{n}}(\boldsymbol{s})$. Further simplifications are possible if both the phases and the amplitudes of n_l, $1 \le l \le N_R$, are mutually independent. In this case, we can express $\Phi_{\hat{\boldsymbol{n}}}(\boldsymbol{s})$ as

$$\Phi_{\hat{\boldsymbol{n}}}(\boldsymbol{s}) = \prod_{l=1}^{N_R}\Phi_{\hat{n}_l}(s_l\Re\{n_l\}), \qquad (7)$$

where only the scalar MGFs $\Phi_{\hat{n}_l}(s) \triangleq \mathcal{E}_{\hat{n}_l}\{e^{-s\Re\{\hat{n}_l\}}\}$ of the elements $\hat{n}_l \triangleq e^{-j\Theta_l}n_l$ of $\hat{\boldsymbol{n}}$ are required. If the phases of the n_l, $1 \le l \le N_R$, are uniformly distributed in $[-\pi, \pi)$, $\Phi_{\hat{n}_l}(s) = \Phi_{n_l}(s) \triangleq \mathcal{E}_{n_l}\{e^{-s\Re\{n_l\}}\}$ is valid, i.e., only the scalar MGFs of the noise components are required.

The scalar MGFs $\Phi_{\hat{n}_l}(s)$ of several practically relevant types of noise are collected in Table 2, cf. Section 5. If $\Phi_{\hat{\boldsymbol{n}}}(\boldsymbol{s})$ cannot be calculated in closed form, it can be computed by numerical integration even if $\Phi_{\hat{\boldsymbol{n}}}(\boldsymbol{s}) = \Phi_{\boldsymbol{n}}(\boldsymbol{s})$ is not valid (i.e., if the phases of n_l, $1 \le l \le N_R$, are not mutually independent and/or are not uniformly distributed in $[-\pi, \pi)$). However, even if closed–form expressions for the MGF are available, calculation of $\Phi_{\Delta(x,z)}(s)$ in closed form is usually not possible, and evaluation of (6) entails N_R numerical integrals.

3.2 Approximate Upper Bound

Assuming a convolutional code of rate $R_c = k_c/n_c$ (k_c and n_c are integers) the union bound for the BER of BICM is given by [1]

$$P_b \leq \frac{1}{k_c} \sum_{d=d_f}^{\infty} w_c(d)\, P(\boldsymbol{c}, \hat{\boldsymbol{c}}), \tag{8}$$

where $\boldsymbol{c}$ and $\hat{\boldsymbol{c}}$ are two distinct code sequences with Hamming distance d that differ only in $l \geq 1$ consecutive trellis states, $w_c(d)$ denotes the total input weight of error events at Hamming distance d, and d_f is the free distance of the code. $P(\boldsymbol{c}, \hat{\boldsymbol{c}})$ is the pairwise error probability (PEP), i.e., the probability that the decoder chooses code sequence $\hat{\boldsymbol{c}}$ when code sequence $\boldsymbol{c} \neq \hat{\boldsymbol{c}}$ is transmitted. Invoking the expurgated bound from [1], the PEP can be expressed as

$$P(\boldsymbol{c}, \hat{\boldsymbol{c}}) = \frac{1}{2\pi j} \int_{c-j\infty}^{c+j\infty} \left(\frac{1}{m_c 2^{m_c}} \sum_{i=1}^{m_c} \sum_{b=0}^{1} \sum_{x \in \mathcal{X}_b^i} \Phi_{\Delta(x,z)}(s) \right)^d \frac{\mathrm{d}s}{s}, \tag{9}$$

where c is a small positive constant that lies in the region of convergence of the integrand. The integral in (9) can be efficiently evaluated numerically using a Gauss–Chebyshev quadrature rule, cf. [28]. Eqs. (8) and (9) constitute an approximate upper bound on the BER and are generalizations of similar bounds in [1, 17] for AWGN to arbitrary types of noise (and interference). We cannot prove that (8) with (9) is a true upper bound since, as has been pointed out in [12], the proof provided in [1] for the expurgated bound is not correct. Nevertheless, our results in Section 6 do suggest that (8) with (9) is an asymptotically tight upper bound if Gray labeling is applied. We note that all our results can be extended to the revised expurgated bounds presented in [12].

4 Asymptotic Analysis

In this section, we analyze the asymptotic behavior of the upper bound in (8) for high SNR, i.e., $\gamma \to \infty$. For this purpose, it is convenient to consider the conditional PEP

$$P(\boldsymbol{c}, \hat{\boldsymbol{c}} \,|\, \boldsymbol{n}) = \frac{1}{2\pi j} \int_{c-j\infty}^{c+j\infty} \Phi(s|\boldsymbol{n}) \frac{\mathrm{d}s}{s}, \tag{10}$$

$$\Phi(s|\boldsymbol{n}) = \left(\frac{1}{m_c 2^{m_c}} \sum_{i=1}^{m_c} \sum_{b=0}^{1} \sum_{x \in \mathcal{X}_b^i} \Phi_{\Delta(x,z)}(s|\boldsymbol{n}) \right)^d, \tag{11}$$

where $\Phi_{\Delta(x,z)}(s|\boldsymbol{n}) = \mathcal{E}_{\boldsymbol{a},\boldsymbol{\Theta}}\{e^{-s\Delta(x,z)}\}$ with channel phase vector $\boldsymbol{\Theta} \triangleq [\Theta_1 \ \dots \ \Theta_{N_R}]^T$. The conditional PEP in (10) is given by the sum of the residues of $\Phi(s|\boldsymbol{n})/s$ at poles lying in the left hand side (LHS) of the complex s–plain (including the imaginary axis) [28]. In order to investigate the singularities of $\Phi(s|\boldsymbol{n})/s$, we derive the Laurent series representation of $\Phi(s|\boldsymbol{n})$ around $s = 0$ for the asymptotic case of $\gamma \to \infty$ in the following subsection.

4.1 Laurent Series Expansion of $\Phi(s|\boldsymbol{n})$

For $\gamma \to \infty$ errors only occur for small channel gains, i.e., for $\boldsymbol{a} \to \boldsymbol{0}_{N_R}$, see also [21]. Exploiting the fact that the elements of $\boldsymbol{a}$ and $\boldsymbol{\Theta}$ are asymptotically i.i.d. for $\gamma \to \infty$, cf. Section 2.2, we can rewrite $\Phi_{\Delta(x,z)}(s|\boldsymbol{n})$ as

$$\Phi_{\Delta(x,z)}(s|\boldsymbol{n}) \overset{\circ}{=} \prod_{l=1}^{N_R} \Phi_{\Delta(x,z)}(s|n_l), \tag{12}$$

where $\Phi_{\Delta(x,z)}(s|n_l) \triangleq \mathcal{E}_{a_l,\Theta_l}\{e^{-s\gamma d_{xz}^2 |a_l|^2} e^{2\sqrt{\gamma}d_{xz} a_l \Re\{\hat{n}_l\} s}\}$. Using the Taylor series expansion $e^x = \sum_{i=0}^{\infty} x^i/i!$, the integral $\int_0^{\infty} x^{\mu-1}e^{-px^2}\,\mathrm{d}x = p^{\mu/2}\Gamma(\mu/2)$ [29, 3.462], and (3), $\Phi_{\Delta(x,z)}(s|n_l)$ can be expressed as

$$\begin{aligned}
\Phi_{\Delta(x,z)}(s|n_l) &= \mathcal{E}_{a_l,\Theta_l}\left\{ e^{-s\gamma d_{xz}^2 |a_l|^2} \sum_{i=0}^{\infty}(2\sqrt{\gamma}d_{xz}\,a_l\Re\{\hat{n}_l\}\,s)^i/i! \right\} \\
&= \frac{\alpha_c}{(\gamma d_{xz}^2 s)^{\alpha_d}} \sum_{i=0}^{\infty} 2^i\Gamma(\alpha_d + i/2)\mathcal{E}_{\Theta_l}\{\Re\{\hat{n}_l\}^i\}s^{i/2} + o\left(\gamma^{-\alpha_d}\right).
\end{aligned} \tag{13}$$

Using $\mathcal{E}_{\Theta_l}\{\Re\{\hat{n}_l\}^i\} = \frac{i/2+1/2}{\sqrt{\pi}\Gamma(i/2+1)}|n_l|^i$, i even, and $\mathcal{E}_{\Theta_l}\{\Re\{\hat{n}_l\}^i\} = 0$, i odd, in (13) leads to

$$\Phi_{\Delta(x,z)}(s|n_l) = \frac{\alpha_c}{(\gamma d_{xz}^2 s)^{\alpha_d}} \sum_{i=0}^{\infty} \beta_i|n_l|^{2i}s^i + o\left(\gamma^{-\alpha_d}\right), \tag{14}$$

where β_i is defined as

$$\beta_i \triangleq \frac{2^{2i}\Gamma(\alpha_d + i)\Gamma(i + 1/2)}{(2i)!\Gamma(i + 1)} = \frac{\Gamma(\alpha_d + i)}{(i!)^2}. \tag{15}$$

The asymptotic Laurent series expansion of $\Phi(s|\boldsymbol{n})$ is obtained from (11), (12), and (14) as

$$\Phi(s|\boldsymbol{n}) = X(\alpha, N_R, d)\,\alpha_c^{N_R d}\,(\gamma s)^{-\alpha_d N_R d}\left(\prod_{l=1}^{N_R} z_l(s)\right)^d + o\left(\gamma^{-\alpha_d N_R d}\right) \tag{16}$$

with $z_l(s) \triangleq \sum_{i=0}^{\infty} \beta_i|n_l|^{2i}s^i$ and modulation dependent constant

$$X(\alpha_d, N_R, d) \triangleq \left(\frac{1}{m_c 2^{m_c}} \sum_{i=1}^{m_c} \sum_{b=0}^{1} \sum_{x \in \mathcal{X}_b^i} \frac{1}{(d_{xz}^2)^{\alpha_d N_R}}\right)^d. \tag{17}$$

In the next subsection, we will use (16) to calculate a closed–form expression for the asymptotic BER.

4.2   Approximation for Asymptotic BER

As mentioned before, the conditional PEP (10) is given by the sum of the residues of $\Phi(s|\boldsymbol{n})/s$ in the LHS of the complex s–plain. Using d'Alembert's convergence test [29, 0.222] it is easy to show that $z_l(s)$ is convergent for all s. Thus, $(\prod_{l=1}^{N_R} z_l(s))^d$ is also convergent for all s. Consequently, the first term on the right hand side (RHS) of (16), which dominates for high SNR, is convergent for $s \neq 0$, i.e., for high SNR the only singularity of $\Phi(s|\boldsymbol{n})/s$ is at $s = 0$. Thus, the asymptotic conditional PEP is given by the residue of $\Phi(s|\boldsymbol{n})/s$ at $s = 0$ or equivalently by the coefficient associated with s^0 in the series expansion of the first term on the RHS of (16). Assuming $\alpha_d N_R d$ is an integer this leads to

$$P(\boldsymbol{c}, \hat{\boldsymbol{c}} \,|\, \boldsymbol{n}) = X(\alpha_d, N_R, d)\, \alpha_c^{N_R d} \gamma^{-\alpha_d N_R d} \sum_{i_1 + \cdots + i_d = \alpha_d N_R d} \prod_{k=1}^{d} \sum_{j_1 + \cdots + j_{N_R} = i_k} \beta_{j_1} |n_1|^{2j_1} \cdots \beta_{j_{N_R}} |n_{N_R}|^{2j_{N_R}}$$
$$+ o\left(\gamma^{-\alpha_d N_R d}\right). \tag{18}$$

Based on (8) and (18) a closed–form approximation for the asymptotic unconditional BER $P_b \overset{\circ}{=} \frac{w_c(d_f)}{k_c}$ $\mathcal{E}\{P(\boldsymbol{c}, \hat{\boldsymbol{c}} \,|\, \boldsymbol{n})\}$ can be obtained as

$$P_b \overset{\circ}{=} \frac{w_c(d_f)}{k_c}\, \alpha_c^{N_R d_f}\, X(\alpha_d, N_R, d_f)\, M(\alpha_d, N_R, d_f)\, \gamma^{-\alpha_d N_R d_f}, \tag{19}$$

where

$$M(\alpha_d, N_R, d) = \sum_{i_1 + \cdots + i_d = \alpha_d N_R d} \prod_{k=1}^{d} \sum_{j_1 + \cdots + j_{N_R} = i_k} \beta_{j_1} \cdots \beta_{j_{N_R}}\, M_{\boldsymbol{n}}(j_1, \ldots, j_{N_R}), \tag{20}$$

with the joint noise moments

$$M_{\boldsymbol{n}}(j_1, \ldots, j_{N_R}) \triangleq \mathcal{E}_{\boldsymbol{n}}\left\{|n_1|^{2j_1} \ldots |n_{N_R}|^{2j_{N_R}}\right\}. \tag{21}$$

In arriving at (19)–(21) we have used the assumptions that (a) the first term in the summation in (8) is asymptotically dominant, (b) the union bound is an accurate approximation for the BER at high SNR, (c) the noise vectors $\boldsymbol{n}$ are i.i.d., and (d) all joint moments of the elements of $\boldsymbol{n}$ exist. Assumption (d) is necessary since the terms absorbed in $o(\gamma^{-\alpha_d N_R d})$ in (18), contain sums of products of elements of $\boldsymbol{n}$, cf. (13), which have been neglected in (19). At what finite SNR the approximate upper bound (10) and the true BER approach the asymptotic BER depends on how fast the terms neglected in

(19) become negligible compared to the terms considered as the SNR increases. Generally, the SNR values at which the asymptotic BER is approached increase with increasing $\alpha_d N_R d_f$ and increasing $w(d_f + 1)/w(d_f)$ since higher SNRs are necessary for the term $w(d_f)\gamma^{-\alpha_d N_R d_f}$ considered in (19) to dominate the largest term $w(d_f + 1)\gamma^{-\alpha_d N_R d_f - 1}$ absorbed in $o(\gamma^{-\alpha_d N_R d})$. Thus, we expect the asymptotic BER to converge faster to the true BER for codes with smaller free distance d_f and smaller relative weight $w(d_f + 1)/w(d_f)$, cf. Fig. 3. Furthermore, depending on the properties of the noise, evaluation of $M_{\boldsymbol{n}}(j_1, \ldots, j_{N_R})$ may be cumbersome. However, for two important special cases significant simplifications are possible.

Case 1 (spatially i.i.d. noise): If the components of $\boldsymbol{n}$ are independent, (20) simplifies to

$$M(\alpha_d, N_R, d) = \sum_{j_1 + \cdots + j_{N_R d} = \alpha_d N_R d} \beta_{j_1} M_n(j_1) \ldots \beta_{j_{N_R d}} M_n(j_{N_R d}) \tag{22}$$

with scalar noise moments $M_n(j) \triangleq \mathcal{E}\{|n_l|^{2j}\}$, which are independent of l.

Case 2 ($\alpha_d = 1$): If $\alpha_d = 1$, which is true for example for (possibly spatially correlated) Rayleigh, Ricean, and Nakagami–q fading, (20) simplifies to

$$M(1, N_R, d) = \frac{1}{(N_R d)!} \sum_{i_1 + \cdots + i_d = N_R d} \binom{N_R d}{i_1, \ldots, i_d} M_{\boldsymbol{n}}(i_1) \ldots M_{\boldsymbol{n}}(i_d) \tag{23}$$

with vector noise moments $M_{\boldsymbol{n}}(i) \triangleq \mathcal{E}\{||\boldsymbol{n}||^{2i}\}$.

Closed–form expressions for the moments $M_n(j)$ and $M_{\boldsymbol{n}}(i)$ of several important types of noise are provided in Tables 2 and 3, respectively, cf. Section 5.

In the remainder of this section, we discuss the implications of the asymptotic BER (19) for system design and consider the special cases of AWGN and uncoded transmission, respectively.

4.3 Diversity Gain, Coding Gain, and Design Guidelines

To get more insight, it is convenient to express the asymptotic BER as $P_b \doteq (G_c \gamma)^{-G_d}$ [21], where G_d and G_c denote the diversity gain (i.e., the asymptotic slope of the BER curve on a double logarithmic scale) and the coding gain (i.e., a relative horizontal shift of the BER curve), respectively. Considering the asymptotic BER in (19), we obtain

$$G_d = \alpha_d N_R d_f \tag{24}$$

$$G_c [\text{dB}] = -\frac{10}{\alpha_d} \log_{10} \alpha_c - \frac{10}{G_d} \log_{10} \left(\frac{w_c(d_f) X(\alpha_d, N_R, d_f)}{k_c} \right) - \frac{10}{G_d} \log_{10} M(\alpha_d, N_R, d_f) \tag{25}$$

From (24) we observe that the diversity gain of BICM is independent of the type of noise. The coding gain in (25) consists of three terms, where the first, the second, and the third term depend on the fading channel, the modulation scheme and the code, and the type of noise, respectively. The primary goal of BICM design is to maximize d_f for a given decoding complexity in order to maximize G_d (and to minimize the asymptotic BER). Gray labelings (yielding smaller $X(\alpha_d, N_R, d_f)$ than non–Gray labelings) and codes with small $w_c(d_f)$ are advantageous for maximizing the second, modulation and coding dependent term in (25). Once d_f is fixed, the last term in (25) cannot be further influenced through system design making the BICM design guidelines effectively indepenent of the type of noise in the system. Thus, our results show that BICM systems optimized based on the guidelines provided in [1] for systems operating in fading and AWGN are also optimum for non–AWGN environments as long as the standard ED branch metric is used for Viterbi decoding.

4.4   Special Case I: AWGN

Although the main focus of this paper is non–AWGN, the presented results are also valid for AWGN. We note that although the AWGN case was covered extensively in the literature, e.g. [1, 13, 17], our results are still more general than existing results as they allow for spatially correlated fading and more general fading models. For example, for Ricean fading ($\alpha_d = 1$) we obtain from (22) with the help of (15) and Table 2 $M(1, N_R, d) = \binom{2N_R d_f - 1}{N_R d_f}$. Thus, with (19) and Table 1 we get

$$P_b \doteq \binom{2N_R d_f - 1}{N_R d_f} \left(\frac{w_c(d_f) \exp\left(-\boldsymbol{\mu}_h^H \boldsymbol{C}_{hh}^{-1} \boldsymbol{\mu}_h\right)}{k_c \det(\boldsymbol{C}_{hh})} \right)^{d_f} X(1, N_R, d_f) \gamma^{-N_R d_f}, \qquad (26)$$

which is a new result. For $N_R = 1$, we may rewrite (26) as $P_b \doteq \binom{2d_f - 1}{d_f} \frac{w_c(d_f)}{k_c} [(1 + K)e^{-K}]^{d_f} X(1, 1, d_f) \gamma^{-d_f}$ with Ricean factor $K \triangleq |\mu_h|^2 / \sigma_h^2$, where μ_h and σ_h^2 denote the mean and the variance of h_1. In contrast, for Ricean fading with $N_R = 1$ the Chernoff bound was used in [1] and [17] to investigate the asymptotic behavior of BICM–SC and BICM–OFDM, respectively, since "a closed–form expression for the PEP for arbitrary K is missing" [1]. Comparing our result with the asymptotic Chernoff bound [1, Eq. (62)] shows that the Chernoff bound is by a factor of $4^{d_f} / \binom{2d_f - 1}{d_f} > 1$ larger than the asymptotic BER, i.e., for $d_f = 3$ and $d_f = 6$ the Chernoff bound is horizontally shifted by 2.7 dB and 1.6 dB compared to the asymptotic BER, respectively. Furthermore, using the Stirling approximation we obtain for the difference between asymptotic Chernoff bound and asymptotic BER $4^{d_f} / \binom{2d_f - 1}{d_f} \to 2\sqrt{\pi d_f}$ for $d_f \gg 1$, which agrees with the result obtained in [16] for Rayleigh fading.

4.5   Special Case II: Uncoded Transmission

While BICM is the main focus of this paper, based on (19) it is also possible to compute the asymptotic BER of uncoded transmission with maximum–ratio combining (MRC) at the receiver. In this case, $d_f = 1$, $k_c = 1$, and $w_c(1) = 1$ are valid. Furthermore, assuming a regular signal constellation such as M–ary quadrature amplitude modulation (M–QAM) or M–ary phase shift keying (M–PSK), it is easy to see that $X(\alpha_d, N_R, 1) = N_{\min}/(m_c d_{\min}^{2\alpha_d N_R})$, where $N_{\min}$ and $d_{\min}$ are the average number of minimum distance neighbors and the minimum distance of $\mathcal{X}$, respectively. Therefore, the asymptotic BER of uncoded transmission with MRC can be expressed as

$$P_b \doteq \frac{N_{\min}\alpha_c^{N_R}}{m_c d_{\min}^{2\alpha_d N_R}} \, M(\alpha_d, N_R, 1) \, \gamma^{-\alpha_d N_R}, \tag{27}$$

where $M(\alpha_d, N_R, 1) = \sum_{j_1+\cdots+j_{N_R}=\alpha_d N_R} \beta_{j_1}\cdots\beta_{j_{N_R}} M_{\boldsymbol{n}}(j_1,\ldots,j_{N_R})$, which can be further simplified for $\alpha_d = 1$ and spatially i.i.d. noise, cf. Section 4.2. In particular, for $\alpha_d = 1$ we obtain $M(1, N_R, 1) = M_{\boldsymbol{n}}(N_R)/N_R!$, cf. (23), and it can be shown that for Rayleigh and Ricean fading (for both of which $\alpha_d = 1$ holds) (27) is identical to [23, Eqs. (12), (16)]. However, (27) is more general than the results in [23] since it is not limited to Rayleigh and Ricean fading and is also applicable to e.g. Nakagami–m, Nakagami–q, and Weibull fading.

5   Calculation of the Noise Moments and MGFs

In this section, we discuss several practically relevant types of noise and compute the corresponding MGFs $\Phi_{\hat{\boldsymbol{n}}}(\boldsymbol{s})$ and moments $M_{\boldsymbol{n}}(j_1,\ldots,j_{N_R})$ required for evaluation of the upper bound in Section 3 and the asymptotic BER in Section 4, respectively. We note that for spatially i.i.d. noise only the scalar MGFs $\Phi_{\hat{n}}(s)$ and the scalar moments $M_n(i)$ have to be computed for evaluation of the upper bound and the asymptotic BER, respectively, cf. (7), (22), Table 2. Furthermore, for most types of spatially dependent noise, it is difficult to find closed–form expressions for the joint MGF $\Phi_{\boldsymbol{n}}(\boldsymbol{s})$ and the joint moments $M_{\boldsymbol{n}}(j_1,\ldots,j_M)$, since the phases of the elements of $\boldsymbol{n}$ are not independent. Therefore, unless stated otherwise, we concentrate in case of spatially dependent noise on the important special cases $\alpha_d = 1$ (with arbitrary N_R) and $N_R = 1$ (with arbitrary α_d), where only the vector moments $M_{\boldsymbol{n}}(i)$ and the scalar moments $M_n(i)$ of the noise are required, respectively.

5.1 Noise Models for BICM–SC

In this section, we consider several time–domain noise models typical for BICM–SC systems. In particular, we consider spatially independent Gaussian–mixture noise (SI–GMN) and three different types of spatially dependent noise (spatially dependent (SD) GMN, additive correlated Gaussian noise (ACGN), and asynchronous co–channel interference (CCI)).

SI–GMN: GMN is often used to model the combined effect of Gaussian background noise and man–made or impulsive noise, cf. e.g. [7, 8, 19]. If the phenomenon causing the impulsive behavior affects the antennas independently, the GMN is spatially i.i.d. [30] and n_l is distributed according to [8]

$$p_n(n_l) = \sum_{i=1}^{I} \frac{c_i}{\pi \sigma_i^2} \exp\left(-\frac{|n_l|^2}{\sigma_i^2}\right), \qquad 1 \le l \le N_R, \tag{28}$$

where $c_i > 0$ and $\sigma_i^2 > 0$ are parameters, and $\sum_{i=1}^{I} c_i \sigma_i^2 = 1$. Two popular special cases of Gaussian mixture noise are Middleton's Class–A noise [8] and ϵ–mixture noise. For ϵ–mixture noise $I = 2$, $c_1 = 1 - \epsilon$, $c_2 = \epsilon$, $\sigma_1^2 = \sigma_g^2$, and $\sigma_2^2 = \kappa \sigma_g^2$, where ϵ is the fraction of time when the impulsive noise is present, κ is the ratio of the variances of the Gaussian background noise and the impulsive noise, and $\sigma_g^2 = 1/(1 - \epsilon + \kappa \epsilon) = 1$. The scalar MGF $\Phi_{\hat{n}}(s)$ and the scalar moments $M_n(i)$ for SI–GMN are given in Table 2.

SD–GMN: SD–GMN is an appropriate model for impulsive noise if all antennas are affected simultaneously by the phenomenon causing the impulsive behavior. The joint pdf for SD–GMN $\boldsymbol{n}$ is given by [30]

$$p_{\boldsymbol{n}}(\boldsymbol{n}) = \sum_{i=1}^{I} \frac{c_i}{\pi^{N_R} \sigma_i^{2N_R}} \exp\left(-\frac{||\boldsymbol{n}||^2}{\sigma_i^2}\right), \tag{29}$$

where c_i and σ_i^2 are defined similarly as for SI–GMN. Since the phases of the elements of $\boldsymbol{n}$ are independent random variables, the joint MGF $\Phi_{\hat{\boldsymbol{n}}}(\boldsymbol{s})$ can be calculated to

$$\Phi_{\hat{\boldsymbol{n}}}(\boldsymbol{s}) = \sum_{i=1}^{I} c_i \exp\left(\frac{\sigma_i^2}{4} \sum_{l=1}^{N_R} s_l^2\right). \tag{30}$$

Furthermore, in this particular case, a closed–form expression for the joint moment $M_{\boldsymbol{n}}(j_1, \ldots, j_{N_R})$, cf. (21), can be obtained as

$$M_{\boldsymbol{n}}(j_1, \ldots, j_{N_R}) = j_1! \cdots j_{N_R}! \sum_{i=1}^{I} c_i \sigma_i^{2(j_1 + \cdots + j_{N_R})}. \tag{31}$$

The vector moments $M_{\boldsymbol{n}}(i)$ are provided in Table 3.

ACGN: In BICM–SC systems, correlated Gaussian noise $\boldsymbol{n}$ may be caused by narrowly spaced receive antennas [6]. Correlated Gaussian interference $\boldsymbol{n} = \tilde{\boldsymbol{h}}b + \tilde{\boldsymbol{n}}$ is caused by a synchronous co–channel interferer transmitting i.i.d. PSK symbols b over a spatially correlated Rayleigh fading channel with gains $\tilde{\boldsymbol{h}}$ and AWGN $\tilde{\boldsymbol{n}}$. In both cases $\boldsymbol{n}$ is fully characterized by its covariance matrix $\boldsymbol{C}_{nn} \triangleq \mathcal{E}\{\boldsymbol{n}\boldsymbol{n}^H\}$, and the corresponding vector moments $M_{\boldsymbol{n}}(i)$ are given in Table 3, where λ_l, $1 \le l \le N_R$, denotes the eigenvalues of $\boldsymbol{C}_{nn}$.

Asynchronous CCI: Another common type of non–AWGN impairment in BICM–SC systems is asynchronous CCI [4, 5]. We consider coding over B different hopping frequencies and assume that at hopping frequency μ, $1 \le \mu \le B$, in addition to AWGN $\tilde{\boldsymbol{n}}_\mu$, there are I_μ Rayleigh faded asynchronous CCI signals leading to time–domain noise

$$\boldsymbol{n}_\mu = \sum_{i=1}^{I_\mu} \tilde{\boldsymbol{h}}_\mu[i] \sum_{l=k_l}^{k_u} g_{i,\mu}[l] b_{i,\mu}[l] + \tilde{\boldsymbol{n}}_\mu, \tag{32}$$

where $\tilde{\boldsymbol{h}}_\mu[i]$ and $b_{i,\mu}[l] \in \mathcal{M}_{i,\mu}$ ($\mathcal{M}_{i,\mu}$: $\tilde{M}_{i,\mu}$–ary symbol alphabet) denote the temporally i.i.d. zero–mean Gaussian random channel vector and the i.i.d. symbols of the ith interferer at the μth hopping frequency, respectively. Furthermore, $g_{i,\mu}[l] \triangleq g_{i,\mu}(lT + \tau_{i,\mu})$, where $g_{i,\mu}(t)$, T, and $\tau_{i,\mu}$ are the effective pulse shape, the symbol duration, and the time offset of the ith interferer at the μth hopping frequency, respectively. We assume that $g_{i,\mu}(lT + \tau_{i,\mu}) \approx 0$ for $i < k_l$ and $i > k_u$, denote the set of all possible values of $\xi_{i,\mu} \triangleq \sum_{l=k_l}^{k_u} g_{i,\mu}[l] b_{i,\mu}[l]$ by $\mathcal{S}_{i,\mu}$, and define $\mathcal{S}_\mu \triangleq \mathcal{S}_{1,\mu} \times \ldots \times \mathcal{S}_{I_\mu,\mu}$. If $I_\mu = 0$, we formally set $\mathcal{S}_\mu = \{0\}$ with $|\mathcal{S}_\mu| = 1$. With these definitions, the pdf of $\boldsymbol{n}_\mu$ can be expressed as

$$p_{\boldsymbol{n}}(\boldsymbol{n}) = \sum_{\mu=1}^{B} \sum_{\mathcal{S}_\mu} \frac{c_{\mu,\mathcal{S}_\mu}}{\pi^{N_R} \det(\boldsymbol{C}_{\mathcal{S}_\mu})} \exp\left(-\boldsymbol{n}^H \boldsymbol{C}_{\mathcal{S}_\mu}^{-1} \boldsymbol{n}\right), \tag{33}$$

where $c_{\mu,\mathcal{S}_\mu} \triangleq 1/(|\mathcal{S}_\mu|B)$ and $\boldsymbol{C}_{\mathcal{S}_\mu} \triangleq \sum_{i=1}^{I_\mu} |\xi_{i,\mu}|^2 \mathcal{E}\{\tilde{\boldsymbol{h}}_\mu[i]\tilde{\boldsymbol{h}}_\mu^H[i]\} + \sigma_{\tilde{n}}^2 \boldsymbol{I}_{N_R}$ ($\sigma_{\tilde{n}}^2$: variance of elements of $\tilde{\boldsymbol{n}}_\mu$). Eq. (33) shows that CCI in BICM–SC systems can be interpreted as correlated Gaussian mixture noise. For future reference we denote the ratio of the total CCI variance and the total AWGN variance by κ, cf. Section 6. The scalar moments $M_n(i)$ (valid for $N_R = 1$) and vector moments $M_{\boldsymbol{n}}(i)$ of asynchronous CCI are given in Tables 2 and 3, respectively, where we have replaced $\boldsymbol{C}_{\mathcal{S}_\mu}$ by $\sigma_{\mathcal{S}_\mu}^2$ for $N_R = 1$ in Table 2, and in Table 3, $\lambda_{l,\mathcal{S}_\mu}$, $1 \le l \le N_R$, are the eigenvalues of $\boldsymbol{C}_{\mathcal{S}_\mu}$.

5.2 Noise Models for BICM–OFDM

Now, we turn our attention to several frequency–domain noise models relevant to BICM–OFDM systems. In particular, we consider SI–GMN and two types of spatially dependent noise (SD–GMN and narrowband interference (NBI)).

SI–GMN: Taking into account that in OFDM systems time domain and frequency domain are linked via the discrete Fourier transform (DFT), it can be shown that time–domain SI–GMN (28) results in frequency–domain noise with pdf

$$p_n(n_l) = \sum_{k_1+\cdots+k_I=N} \frac{c_{k_1,\ldots,k_I}}{\pi \sigma^2_{k_1,\ldots,k_I}} \exp\left(-\frac{|n_l|^2}{\sigma^2_{k_1,\ldots,k_I}}\right), \qquad 1 \le l \le N_R, \tag{34}$$

which is again an SI–GMN model with parameters $c_{k_1,\ldots,k_I} \triangleq \binom{N}{k_1,\ldots,k_I} c_1^{k_1} \cdots c_I^{k_I}$ and $\sigma^2_{k_1,\ldots,k_I} \triangleq (k_1\sigma_1^2 + \cdots + k_I\sigma_I^2)/N$. We note that the spectral i.i.d. asumption for n_l is justified only if the interleaver spans several OFDM symbols, i.e., $B \gg 1$, since the noise after DFT in one OFDM symbol will be spectrally dependent. The scalar MGF $\Phi_{\hat{n}}(s)$ and the scalar moments $M_n(i)$ for SI–GMN are provided in Table 2.

SD–GMN: The DFT operation at the receiver transforms the noise pdf (29) into

$$p_n(\boldsymbol{n}) = \sum_{k_1+\cdots+k_I=N} \frac{c_{k_1,\ldots,k_I}}{\pi^{N_R} \sigma^{2N_R}_{k_1,\ldots,k_I}} \exp\left(-\frac{||\boldsymbol{n}||^2}{\sigma^2_{k_1,\ldots,k_I}}\right), \tag{35}$$

where the same definition is used for $c_{k_1,\ldots,k_I}$ and $\sigma^2_{k_1,\ldots,k_I}$ as for SI–GMN, cf. (34). Since, similar to the BICM–SC case, the phases of the elements of $\boldsymbol{n}$ are independent random variables, the joint MGF can be obtained as

$$\Phi_{\hat{n}}(\boldsymbol{s}) = \sum_{k_1+\cdots+k_I=N} c_{k_1,\ldots,k_I} \exp\left(\frac{\sigma^2_{k_1,\ldots,k_I}}{4} \sum_{l=1}^{N_R} s_l^2\right). \tag{36}$$

The corresponding joint moment is given by

$$M_{\boldsymbol{n}}(j_1,\ldots,j_{N_R}) = j_1! \cdots j_{N_R}! \sum_{k_1+\cdots+k_I=N} c_{k_1,\ldots,k_I} \sigma^{2(j_1+\cdots+j_{N_R})}_{k_1,\ldots,k_I}. \tag{37}$$

The vector moments $M_{\boldsymbol{n}}(i)$ for SD–GMN are provided in Table 3.

NBI: We consider a BICM–OFDM system with coding over B different hopping frequencies. At hopping frequency μ, $1 \le \mu \le B$, the received frequency–domain signal is impaired by AWGN $\tilde{\boldsymbol{n}}_{k,\mu}$ and I_μ Rayleigh faded PSK NBI signals. The corresponding frequency–domain noise model is

$$\boldsymbol{n}_{k,\mu} = \sum_{i=1}^{I_\mu} g_{k,\mu}[i] b_\mu[i] \tilde{\boldsymbol{h}}_{k,\mu}[i] + \tilde{\boldsymbol{n}}_{k,\mu}, \qquad 1 \le k \le N, \tag{38}$$

where $b_\mu[i]$ is the PSK symbol of the ith interferer at the μth hopping frequency affecting the set $\mathcal{N}_{\mu,i}$ of sub–carriers via $g_{k,\mu}[i] \triangleq \exp[-j\pi(N-1)(k+f_{\mu,i}/\Delta f_s)/N+\phi_{\mu,i}]\sin[\pi(k+f_{\mu,i}/\Delta f_s)]/\sin[\pi(k+f_{\mu,i}/\Delta f_s)/N]$ [3]. Here, $f_{\mu,i}$ and $\phi_{\mu,i}$ denote the frequency and phase of the ith interferer at hopping frequency μ relative to the user, respectively, and Δf_s is the OFDM sub–carrier spacing. Since we consider NBI, the same interference fading vector $\tilde{\boldsymbol{h}}_{k,\mu}[i]$ (modeled as spatially correlated zero–mean Gaussian random vector) affects all sub–carriers in $\mathcal{N}_{\mu,i}$. For $f_{\mu,i} = \nu\Delta f$, the NBI affects only sub–carrier ν, i.e., $\mathcal{N}_{\mu,i} = \nu$, while, in theory, for $f_{\mu,i} \neq \nu\Delta f$ the NBI affects all sub–carriers. However, $g_{k,\mu}[i]$ decays quickly and we limit $\mathcal{N}_{\mu,i}$ such that $|g_{k,\mu}[i]| \approx 0$ for $k \notin \mathcal{N}_{\mu,i}$. Finally, we assume that no sub–carrier is affected by two narrowband interferers at a given hopping frequency, i.e., $\mathcal{N}_{\mu,i_1} \cap \mathcal{N}_{\mu,i_2} = \emptyset$, $i_1 \neq i_2$. The pdf for this general interference scenario is given by

$$p_{\boldsymbol{n}}(\boldsymbol{n}) = \sum_{\mu=1}^{B}\sum_{i=1}^{I_\mu}\sum_{k\in\mathcal{N}_{\mu,i}}\frac{c_0}{\pi^{N_R}\det(\boldsymbol{C}_{\mu,i,k})}\exp\left(-\boldsymbol{n}^H\boldsymbol{C}_{\mu,i,k}^{-1}\boldsymbol{n}\right) + \frac{c_1}{\pi^{N_R}\sigma_{\tilde{n}}^{2N_R}}\exp\left(-\frac{||\boldsymbol{n}||^2}{\sigma_{\tilde{n}}^2}\right), \quad (39)$$

where $\sigma_{\tilde{n}}^2$ denotes the variance of the elements of the AWGN $\tilde{\boldsymbol{n}}$, $c_0 \triangleq 1/(BN)$, $c_1 \triangleq 1 - \sum_{\mu=1}^{B}\sum_{i=1}^{I_\mu}|\mathcal{N}_{\mu,i}|/(BN)$, $\boldsymbol{C}_{\mu,i,k} \triangleq |g_{k,\mu}[i]|^2\boldsymbol{C}_{\mu,i}+\sigma_{\tilde{n}}^2\boldsymbol{I}_{N_R}$, and $\boldsymbol{C}_{\mu,i} \triangleq \mathcal{E}\{\tilde{\boldsymbol{h}}_{k,\mu}[i](\tilde{\boldsymbol{h}}_{k,\mu}[i])^H\}$. Eq. (39) shows that, similar to CCI in BICM–SC systems, NBI in BICM–OFDM systems can be interpreted as correlated Gaussian mixture noise. We denote the ratio of the total NBI variance and the AWGN variance by κ, cf. Section 6. The corresponding moments $M_n(i)$ and $M_{\boldsymbol{n}}(i)$ are provided in Tables 2 and 3, respectively, where we have replaced $\boldsymbol{C}_{\mu,i,k}$ by $\sigma_{\mu,i,k}^2$ for $N_R = 1$ in Table 2, and in Table 3, $\lambda_{l,\mu,i,k}$, $1 \leq l \leq N_R$, are the eigenvalues of $\boldsymbol{C}_{\mu,i,k}$.

5.3 Monte–Carlo Method

For complicated types of noise such as UWB interference, it may be difficult to calculate the moments $M_n(i)$, $M_{\boldsymbol{n}}(i)$, and $M_{\boldsymbol{n}}(j_1, \ldots, j_{N_R})$ in closed form. In this case, these moments may be obtained by Monte–Carlo simulation of (21), (22), or (23) and subsequently be used in (19) for calculation of the asymptotic BER. We note that this semi–analytical approach is much faster than a full simulation since the moments are independent from the SNR γ and have to be computed only once.

6   Numerical and Simulation Results

In this section, we verify our derivations in Sections 3–5 with computer simulations and employ the presented theoretical framework to study the performance of BICM in non–AWGN environments. For the simulations, we consider both idealized channels with temporally i.i.d. channel and noise vectors, and non–ideal channels generated based on the models presented in Sections 2.1 and 5. In the non–ideal case, for BICM–SC we assume a frame size of $N = 972$ and a normalized fading bandwidth $B_f T$ of 0.007, which are typical values for the DAMPS mobile communication system [4]. For BICM–OFDM we consider systems with $N = 64$ and $N = 128$ sub–carriers transmitting over channels with $L = 10$ and $L = 20$ i.i.d. impulse response coefficients. For all simulations shown, a pseudo–random interleaver was employed. Throughout this section we adopt the standard convolutional code with rate $R_c = 1/2$ and generator polynomials [133, 171] (octal representation). Higher code rates are obtained via puncturing and, unless specified otherwise, 4–PSK modulation and $N_R = 1$ receive antennas are used. The parameters of the adopted noise models are specified in the respective captions of Figs. 1–7.

In Fig. 1, we show simulation results for BICM–SC and BICM–OFDM impaired by GMN and NBI, respectively. In both cases, coding $(R_c = 3/4)$ and interleaving is performed over different numbers of frames B. Besides the simulation results we also show the approximate upper bound and the asymptotic BER derived in Sections 3 and 4, respectively. For high enough SNR and BICM–OFDM with $N = 128$ and the severely frequency–selective channel with $L = 20$ the analytical results are accurate even for $B = 3$. In contrast, for BICM–SC and BICM–OFDM with $N = 64$ and $L = 10$ the interleaver is not able to generate i.i.d. channels for small B which leads to performance degradation and the corresponding simulated BER exceeds the upper bound (which was derived assuming i.i.d. channels). However, as B increases, the simulation results approach the upper bound and the asymptotic BER also in these cases for high SNR. Note that for non–delay critical applications, such as data transmission, large B can be afforded.

In Fig. 2, we show the BER of BICM–SC and BICM–OFDM ($N = 64$) for Rayleigh fading and various different noise and interference scenarios. Fig. 2 shows that the simulated BERs (solid lines with markers), which were generated with non–ideal channels and for different B, approach the approximate upper bound (solid lines without markers) and the asymptotic BER (dashed lines) for high SNR. In particular, for the BER region of $\text{BER} < 10^{-5}$, which is difficult to simulate, the

proposed analytical results are accurate approximations for the true BER. The simulated BER exceeds the upper bound again because of the non–ideal channel. In accordance with our findings in Section 4.3, Fig. 2 shows that for high SNR all BER curves are parallel, i.e., all considered types of noise lead to the same diversity gain of $G_d = d_f = 5$. Nevertheless, there are large performance differences between different types of noise because of the different coding gains G_c. Fig. 2 confirms that OFDM is far more robust to GMN than SC if BICM is used in both cases. For GMN II BICM–OFDM outperforms BICM–SC by 5 dB at high SNR and approaches the performance in AWGN. This is an interesting result, since a previous comparison in [19] had shown that BICM–SC is more robust to GMN than *uncoded* OFDM. Note, however, that for BICM–OFDM a relative large B is necessary to make the GMN approximately spectrally independent, whereas for BICM–SC GMN is temporally independent even for $B = 1$, cf. Section 5.

In the remaining figures, we assume ideal channels where both fading and noise are temporally or spectrally i.i.d.

In Fig. 3, we investigate the effect of the code rate R_c on the performance of BICM–OFDM ($N = 128$) in NBI for an i.i.d. Rayleigh fading channel and 64–QAM. Fig. 3 shows that as the code rate decreases, the diversity gain increases since the free distance of the code increases, cf. (24). While the approximate upper bound (solid line without markers) approaches the simulation results (solid lines with markers) for $\text{BER} < 10^{-6}$ in all cases, the convergence of the upper bound to the asymptotic BER (dashed lines) is slower for small ($R_c = 1/2$) and large ($R_c = 7/8$) code rates. For $R_c = 1/2$, d_f is large making the asymptotic BER curve very steep, which leads to an over–estimation of the BER at low SNRs, cf. Section 4.2. For $R_c = 7/8$, the slow convergence can be explained by the large relative weight of terms neglected in asymptotic BER expressions (e.g. $w(d_f + 1)/w(d_f) = 56$), cf. Section 4.2. For comparison, $R_c = 3/4$ shows a much faster convergence since $w(d_f + 1)/w(d_f) = 5$.

In Fig. 4, we consider the impact of the type of fading on the BER of BICM–SC with 16–QAM for GMN and AWGN. Since the type of fading affects the diversity gain $G_d = \alpha_d d_f$, the asymptotic slopes of the BER curves for Nakagami–m ($\alpha_d = m = 2$) and Weibull ($\alpha_d = c/2 = 2/3$) fading differ from the asymptotic slopes of the BER curves for Rayleigh, Ricean, and Nakagami–q fading, since for the latter three $\alpha_d = 1$ holds. It can also be observed that the performance loss caused by GMN compared to AWGN decreases with decreasing diversity order.

In Fig. 5, we show the BERs of *uncoded* SC transmission over correlated Nakagami–m channels with $N_R = 2$ receive antennas and impairment by SD- and SI–GMN (both cases: ϵ–mixture noise

with $\epsilon = 0.1$, $\kappa = 10$). The spatial fading correlation coefficient is $\rho_a = 0.9$. Note that for uncoded transmission the temporal i.i.d. asumption for fading and noise is not required. Fig. 5 shows that for uncoded transmission the derived approximate upper bound is very tight even at low SNR and approaches the asymptotic BER at high SNR. Thereby, the asymptotic BER converges faster to the upper bound for channels with smaller diversity gain. Furthermore, Fig. 5 confirms that spatial noise dependencies lead to significant performance degradations.

In Fig. 6, we consider the BER of BICM–SC impaired by temporally i.i.d., spatially uncorrelated/correlated (fading correlation $\rho_h = 0.9$) Rayleigh fading and AWGN/ACGN (noise correlation $\rho_n = 0.9$) for $N_R = 2$. Fig. 6 shows that, while noise correlation has also adverse effects on performance, fading correlation is more harmful. Furthermore, the convergence of the asymptotic BER to the approximate union bound is negatively affected by the spatial fading correlation.

Finally, in Fig. 7, we consider the BER of BICM–OFDM impaired by UWB interference and temporally i.i.d. Rayleigh fading. We consider MB–OFDM and impulse–radio UWB (IR–UWB) interference following the EMCA [9] and the IEEE 802.15.4a [10] standards, respectively. Specifically, for IR–UWB we assume $N_b = 32$ bursts per symbol and L_c chips per burst [10]. The MGF required for the approximate upper bound (8) was obtained using the methods proposed in [11]. Since, due to the complicated nature of the interference signal, closed–form expressions for the moments are difficult to obtain, we used the Monte–Carlo approach discussed in Section 5.3 for calculation of the moments for evaluation of the asymptotic BER (19). Fig. 7 nicely illustrates that the coding gain in UWB interference strongly depends on the sub–carrier spacing of the victim BICM–OFDM system and the format of the UWB interference. Interestingly, for $\Delta f_s = 100$ MHz MB–OFDM has a more favorable noise pdf than AWGN and thus, is less detrimental to the performance of the BICM–OFDM system than AWGN.

7   Conclusions

In this paper, we have presented a framework for performance analysis of BICM–SC and BICM–OFDM systems impaired by fading and non–Gaussian noise and interference. The proposed analysis is very general and applicable to all popular fading models (including Rayleigh, Ricean, Nakagami–m, Nakagami–q, and Weibull fading) and all types of noise with finite moments (including AWGN, ACGN, GMN, CCI, NBI, and UWB interference). In particular, we have derived an approximate upper

bound for the BER which allows for efficient numerical evaluation and a simple, accurate closed–form approximation for the asymptotic BER. Our asymptotic analysis reveals that while the coding gain is strongly noise dependent, the diversity gain of the overall system is not affected by the type of noise. This result is important from a practical point of view since it shows that at high SNRs the BER curves of BICM systems optimized for AWGN will only suffer from a parallel shift if the impairment in a real–world environment is non–Gaussian.

A   Spatially Correlated Fading Channels

In this appendix, we prove (2) for correlated Rayleigh, Ricean, and Nakagami–m fading.

Ricean Fading: For Ricean fading the pdf of the channel vector $\boldsymbol{h}$ is given by

$$p_{\boldsymbol{h}}(\boldsymbol{h}) = \frac{1}{\pi^{N_R} \det(\boldsymbol{C}_{hh})} \exp\left[-(\boldsymbol{h} - \boldsymbol{\mu}_h)^H \boldsymbol{C}_{hh}^{-1}(\boldsymbol{h} - \boldsymbol{\mu}_h)\right], \tag{40}$$

where $\boldsymbol{\mu}_h \triangleq \mathcal{E}\{\boldsymbol{h}\}$ and $\boldsymbol{C}_{hh} \triangleq \mathcal{E}\{(\boldsymbol{h} - \boldsymbol{\mu}_h)(\boldsymbol{h} - \boldsymbol{\mu}_h)^H\}$ are the channel mean and channel covariance matrix, respectively. For $\boldsymbol{h} \to \boldsymbol{0}_{N_R}$ we can rewrite (40) as

$$p_{\boldsymbol{h}}(\boldsymbol{h}) = \frac{\exp\left(-\boldsymbol{\mu}_h^H \boldsymbol{C}_{hh}^{-1} \boldsymbol{\mu}_h\right)}{\pi^{N_R} \det(\boldsymbol{C}_{hh})} + o(1). \tag{41}$$

Based on (41) and the relation $|h_l|^2 = a_l^2$ it can be shown that (2) and (3) hold for correlated Rayleigh ($\boldsymbol{\mu}_h = \boldsymbol{0}_{N_R}$) and Ricean ($\boldsymbol{\mu}_h \neq \boldsymbol{0}_{N_R}$) fading with α_c and α_d as specified in Table 1.

Nakagami–m Fading: For Nakagami–m fading the joint MGF of a_l^2, $1 \leq l \leq N_R$, is given by [24]

$$\Phi_{\boldsymbol{a}^2}(\boldsymbol{s}) \triangleq \mathcal{E}\left\{\exp\left(-\sum_{l=1}^{N_R} a_l^2 s_l\right)\right\} = \det(\boldsymbol{I}_{N_R} + \boldsymbol{S}\boldsymbol{C}_{aa}/m)^{-m}, \tag{42}$$

where $\boldsymbol{S} \triangleq \operatorname{diag}\{\boldsymbol{s}\}$, and $\boldsymbol{C}_{aa}$ and m denote the channel correlation matrix and the fading parameter, respectively. The behavior of the joint pdf $p_{\boldsymbol{a}^2}(a_1^2, \ldots, a_{N_R}^2)$ of a_l^2, $1 \leq l \leq N_R$, for $\boldsymbol{a} \to \boldsymbol{0}_{N_R}$ can be deduced from the behavior of $\Phi_{\boldsymbol{a}^2}(\boldsymbol{s})$ for $s_l \to \infty$, $1 \leq l \leq N_R$, which is given by

$$\Phi_{\boldsymbol{a}^2}(\boldsymbol{s}) = m^{N_R m} \det(\boldsymbol{C}_{aa})^{-m} \prod_{l=1}^{N_R} s_l^{-m} + o\left(\prod_{l=1}^{N_R} s_l^{-m}\right). \tag{43}$$

Consequently, we obtain

$$p_{\boldsymbol{a}^2}(a_1^2, \ldots, a_{N_R}^2) = m^{N_R m} \det(\boldsymbol{C}_{aa})^{-m} \prod_{l=1}^{N_R} \frac{a_l^{2(m-1)}}{\Gamma(m)} + o\left(\prod_{l=1}^{N_R} a_l^{2(m-1)}\right), \tag{44}$$

which clearly shows that the a_l, $1 \leq l \leq N_R$, are asymptotically i.i.d., i.e., (2) and (3) are valid. The corresponding parameters α_c and α_d are provided in Table 1 and can be obtained by exploiting the relation between $p_{\boldsymbol{a}^2}(a_1^2, \ldots, a_{N_R}^2)$ and $p_{\boldsymbol{a}}(\boldsymbol{a})$.

References

[1] G. Caire, G. Taricco, and E. Biglieri. Bit–Interleaved Coded Modulation. *IEEE Trans. Inform. Theory*, 44:927–946, May 1998.

[2] H. Bölcskei. MIMO–OFDM Wireless Systems: Basics, Perspectives, and Challenges. *IEEE Wireless Commun.*, 13:31–37, August 2006.

[3] A. Coulson. Bit Error Rate Performance of OFDM in Narrowband Interference with Excission Filtering. *IEEE Trans. Wireless Commun.*, 5:2484–2492, September 2006.

[4] T.S. Rappaport. *Wireless Communications*. Prentice Hall, Upper Saddle River, NJ, 2002.

[5] A. Giorgetti and M. Chiani. Influence of Fading on the Gaussian Approximation for BPSK and QPSK with Asynchronous Cochannel Interference. *IEEE Trans. Wireless Commun.*, 4:384–389, March 2005.

[6] S. Krusevac, P. Rapajic, and R. Kennedy. Channel Capacity Estimation for MIMO Systems with Correlated Noise. In *Proceedings of IEEE Global Telecom. Conf.*, pages 2812–2816, Dec. 2005.

[7] R. Prasad, A. Kegel, and A. de Vos. Performance of Microcellular Mobile Radio in a Cochannel Interference, Natural, and Man-Made Noise Environment. *IEEE Trans. Veh. Technol.*, 42:33–40, February 1993.

[8] D. Middleton. Statistical-physical Models of Man–made Radio Noise – Parts I and II. *U.S. Dept. Commerce Office Telecommun.*, April 1974 and 1976.

[9] ECMA. Standard ECMA-368: High Rate Ultra Wideband PHY and MAC Standard. *[Online] http://www.ecma-international.org/publications/standards/Ecma-368.htm*, December 2005.

[10] IEEE P802.15.4a. Wireless Medium Access Control (MAC) and Physical Layer (PHY) Specifications for Low-Rate Wireless Personal Area Networks (LR-WPANs). January 2007.

[11] A. Nasri, R. Schober, and L. Lampe. Performance Evaluation of BICM-OFDM Systems Impaired by UWB Interference. In *Proceedings of IEEE Intern. Commun. Conf. (ICC)*, July 2008.

[12] V. Sethuraman and B. Hajek. Comments on "Bit–Interleaved Coded Modulation". *IEEE Trans. Inform. Theory*, 52:1795–1797, April 2006.

[13] P.-C. Yeh, S. Zummo, and W. Stark. Error Probability of Bit–Interleaved Coded Modulation in Wireless Environments. *IEEE Trans. Veh. Technol.*, 55:722–728, March 2006.

[14] E. Akay and E. Ayanoglu. Achieving Full Frequency and Space Diversity in Wireless Systems via BICM, OFDM, STBC, and Viterbi Decoding. *IEEE Trans. Commun.*, 54:2164–2172, December 2006.

[15] A. Martinez, A. Guillen i Fabregas, and G. Caire. Error Probability Analysis of Bit–Interleaved Coded Modulation. *IEEE Trans. Inform. Theory*, 52:262–271, January 2006.

[16] A. Martinez, A. Guillen i Fabregas, and G. Caire. A Closed–Form Approximation for the Error Probability of BPSK Fading Channels. *IEEE Trans. Wireless Commun.*, 6:2051–2054, June 2007.

[17] D. Rende and T. Wong. Bit–Interleaved Space–Frequency Coded Modulation for OFDM Systems. *IEEE Trans. Wireless Commun.*, 4:2256–2266, September 2005.

[18] Y. Li and J. Moon. Error Probability Bounds for Bit–Interleaved Space–Time Trellis Coding Over Block–Fading Channels. *IEEE Trans. Inform. Theory*, 53:4285–4292, November 2007.

[19] H. Nguyen and T. Bui. Bit–Interleaved Coded Modulation With Iterative Decoding in Impulsive Noise. *IEEE Trans. Power Delivery*, 22:151–160, January 2007.

[20] H. Abdel-Ghaffar and S. Pasupathy. Asymptotic Performance of M-ary and Binary Signals Over Multipath/Multichannel Rayleigh and Ricean Fading. *IEEE Trans. Commun.*, 43:2721–2731, November 1995.

[21] Z. Wang and G. Giannakis. A Simple and General Parameterization Quantifying Performance in Fading Channels. *IEEE Trans. Commun.*, 51:1389–1398, August 2003.

[22] A. Nasri, R. Schober, and Y. Ma. Unified Asymptotic Analysis of Linearly Modulated Signals in Fading, Non–Gaussian Noise, and Interference. *IEEE Trans. Commun.*, 56:980–990, June 2008.

[23] A. Nezampour, A. Nasri, R. Schober, and Y. Ma. Asymptotic BEP and SEP of Quadratic Diversity Combining Receivers in Correlated Ricean Fading, Non–Gaussian Noise, and Interference. *To appear in IEEE Trans. Commun. [Online] http://www.ece.ubc.ca/∼alinezam/TCOM-07.pdf*, 2008.

[24] M.K. Simon and M.-S. Alouini. *Digital Communication over Fading Channels*. Wiley, Hoboken, New Jersey, 2005.

[25] O.C. Ugweje and V.A. Aalo. Performance of Selection Diversity System in Correlated Nakagami Fading. In *Proceedings of IEEE Veh. Techn. Conf. (VTC)*, pages 1488–1492, May 1997.

[26] C. Tan and N. Beaulieu. Infinite Series Representations of the Bivariate Rayleigh and Nakagami-m Distributions. *IEEE Trans. Commun.*, 45:1159–1161, October 1997.

[27] G.A. Tsihrintzis and C.L. Nikias. Performance of Optimum and Suboptimum Receivers in the Presence of Impulsive Noise Modeled as an Alpha-Stable Process. *IEEE Trans. Commun.*, 43:904–914, Feb./Mar./Apr. 1995.

[28] E. Biglieri, G. Caire, G. Taricco, and J. Ventura-Traveset. Computing Error Probabilities over Fading Channels: a Unified Approach. *European Trans. Telecommun.*, 9:15–25, Jan./Feb. 1998.

[29] I. Gradshteyn and I. Ryzhik. *Table of Integrals, Series, and Products*. Academic Press, New York, 2000.

[30] C. Tepedelenlioglu and P. Gao. On Diversity Reception Over Fading Channels with Impulsive Noise. *IEEE Trans. Veh. Technol.*, 54:2037–2047, November 2005.

Tables and Figures:

Table 1: Pdf $p_a(a)$ of fading amplitude a for popular fading models and corresponding values for α_c and α_d. We have omitted subscript l for convenience. The parameters for Rayleigh ($\boldsymbol{C}_{hh}$), Ricean ($\boldsymbol{\mu}_h$, $\boldsymbol{C}_{hh}$), and Nakagami–m (m, $\boldsymbol{C}_{aa}$) fading are defined in Appendix A. The parameters for Nakagami–q (q, b) and Weibull (c) fading are defined as in [24].

Channel type	$p_a(a)$ of the fading amplitude a	α_c	α_d
Rayleigh	$2\,a\,e^{-a^2}$	$\det(\boldsymbol{C}_{hh})^{-1/N_R}$	1
Ricean	$2(K+1)\,a\,e^{-K-(1+K)a^2}\,\mathrm{I}_0\left(2a\sqrt{K(K+1)}\right)$	$\left(\dfrac{\exp\left(-\boldsymbol{\mu}_h^H\boldsymbol{C}_{hh}^{-1}\boldsymbol{\mu}_h\right)}{\det(\boldsymbol{C}_{hh})}\right)^{1/N_R}$	1
Nakagami–m	$\frac{2}{\Gamma(m)}\,m^m\,a^{2m-1}\,e^{-ma^2}$	$\frac{m^m}{\Gamma(m)}\,\det(\boldsymbol{C}_{aa})^{-m/N_R}$	m
Nakagami–q	$\frac{2a}{\sqrt{1-b^2}}\,\exp\left(-\frac{a^2}{(1-b^2)}\right)\,\mathrm{I}_0\left(\frac{ba^2}{(1-b^2)}\right)$	$\frac{1+q^2}{2q}$	1
Weibull	$c\left(\Gamma(1+\frac{2}{c})\right)^{\frac{c}{2}}a^{c-1}\exp\left(-\left(a^2\Gamma(1+\frac{2}{c})\right)^{\frac{c}{2}}\right)$	$\frac{c}{2}\left(\Gamma(1+\frac{2}{c})\right)^{\frac{c}{2}}$	$\frac{c}{2}$

Table 2: MGF $\Phi_{\hat{n}}(s)$ and scalar moments $M_n(i)$ of types of noise considered in Section 5. All variables in this table are defined in Section 5. (SC) and (OFDM) means that the type of noise is relevant for BICM–SC and BICM–OFDM, respectively.

Noise type	Noise MGF $\Phi_{\hat{n}}(s)$	Scalar moment $M_n(i)$
AWGN (SC & OFDM)	$\exp(s^2/4)$	$i!$
GMN (SC)	$\sum_{k=1}^{I} c_k\,\exp(s^2\sigma_k^2/4)$	$i!\sum_{k=1}^{I} c_k\,\sigma_k^{2i}$
CCI (SC)	$\sum_{\mu=1}^{B}\sum_{\mathcal{S}_\mu} c_{\mu,\mathcal{S}_\mu}\,\exp(s^2\sigma_{\mathcal{S}_\mu}^2/4)$	$i!\sum_{\mu=1}^{B}\sum_{\mathcal{S}_\mu} c_{\mu,\mathcal{S}_\mu}\sigma_{\mathcal{S}_\mu}^{2i}$
GMN (OFDM)	$\sum_{k_1+\cdots+k_I=N} c_{k_1,\ldots,k_I}\,\exp(s^2\sigma_{k_1,\ldots,k_I}^2/4)$	$i!\sum_{k_1+\cdots+k_I=N} c_{k_1,\ldots,k_I}\,\sigma_{k_1,\ldots,k_I}^{2i}$
NBI (OFDM)	$\sum_{\mu=1}^{B}\sum_{i=1}^{I_\mu}\sum_{k\in\mathcal{N}_{\mu,i}} c_0\,\exp(s^2\sigma_{\mu,i,k}^2/4)$ $+c_1\,\exp(s^2\sigma_{\tilde{n}}^2/4)$	$i!(\sum_{\mu=1}^{B}\sum_{\nu=1}^{I_\mu}\sum_{k\in\mathcal{N}_{\mu,\nu}} c_0\sigma_{\mu,\nu,k}^{2i}$ $+c_1\sigma_{\tilde{n}}^{2i})$

Table 3: Vector moments $M_{\boldsymbol{n}}(i)$ of types of noise considered in Section 5. All variables in this table are defined in Section 5. (SC) and (OFDM) means that the type of noise is relevant for BICM–SC and BICM–OFDM, respectively.

Noise type	Vector moment $M_{\boldsymbol{n}}(i)$
GMN (SC)	$\frac{(i+N_R-1)!}{(N_R-1)!} \sum_{k=1}^{I} c_k\, \sigma_k^{2i}$
ACGN (SC)	$i! \sum_{k_1+\cdots+k_{N_R}=i} \lambda_1^{k_1} \cdots \lambda_{N_R}^{k_{N_R}}$
CCI (SC)	$i! \sum_{\mu=1}^{B} \sum_{\mathcal{S}_\mu} c_{\mu,\mathcal{S}_\mu} \sum_{k_1+\cdots+k_{N_R}=i} \lambda_{1,\mathcal{S}_\mu}^{k_1} \cdots \lambda_{N_R,\mathcal{S}_\mu}^{k_{N_R}}$
GMN (OFDM)	$\frac{(i+N_R-1)!}{(N_R-1)!} \sum_{k_1+\cdots+k_I=N} c_{k_1,\ldots,k_I}\, \sigma_{k_1,\ldots,k_I}^{2i}$
NBI (OFDM)	$i! \sum_{\mu=1}^{B} \sum_{\nu=1}^{I_\mu} \sum_{k \in \mathcal{N}_{\mu,\nu}} c_0 \sum_{k_1+\cdots+k_{N_R}=i} \lambda_{1,\mu,\nu,k}^{k_1} \cdots \lambda_{N_R,\mu,\nu,k}^{k_{N_R}}$ $+c_1 \frac{(i+N_R-1)!}{(N_R-1)!} \sigma_{\tilde{n}}^{2i}$
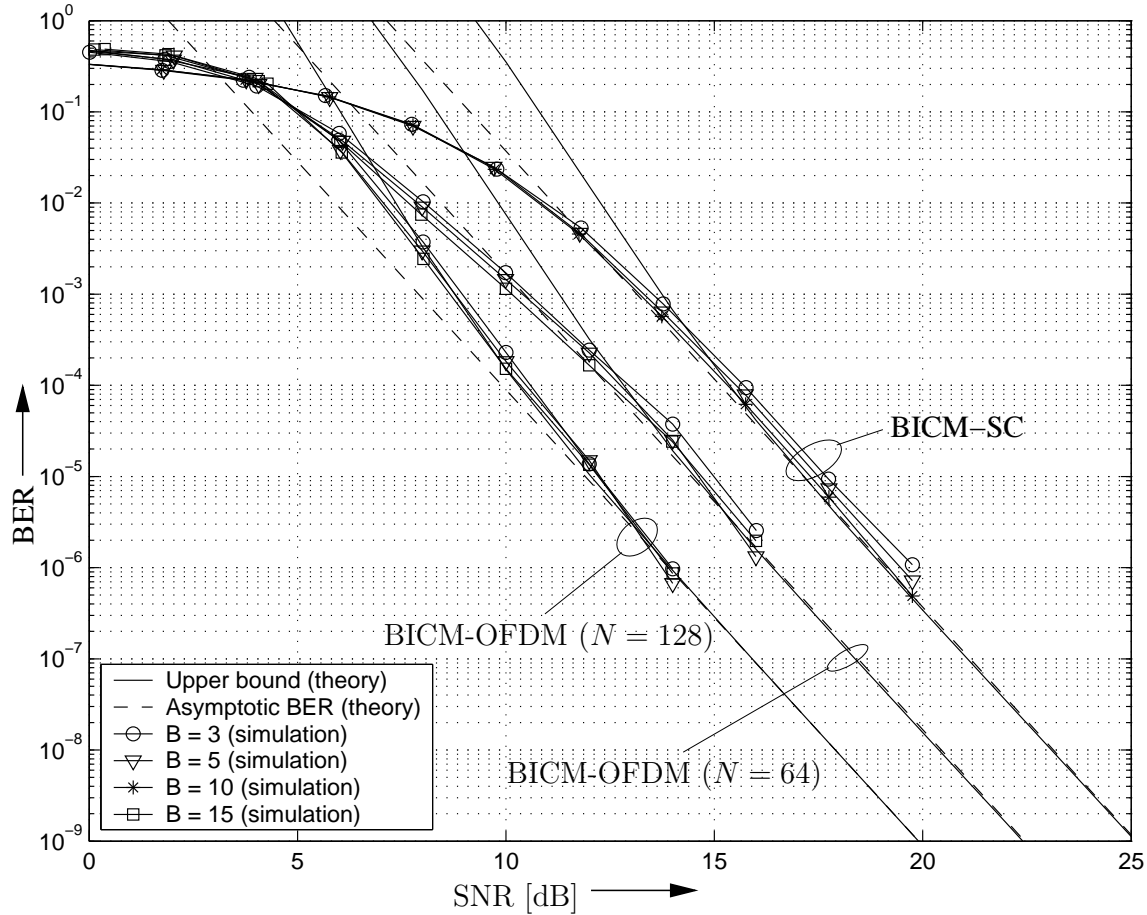
Figure 1: BER of BICM–SC and BICM–OFDM impaired by GMN (ϵ–mixture noise, $\epsilon = 0.1$, $\kappa = 100$) and NBI, respectively, vs. SNR γ. $R_c = 3/4$, Rayleigh fading, 4–PSK, and $N_R = 1$. BICM–SC: Flat time–selective fading, $N = 972$, and $B_f T = 0.007$. BICM–OFDM ($N = 64$): Frequency–selective Rayleigh fading with $L = 10$ and B equal power, sub–carrier centered NBI signals with $I_\mu = 1$, $1 \leq \mu \leq B$, $\kappa = 7$. BICM–OFDM ($N = 128$): Frequency–selective Rayleigh fading with $L = 20$ and B equal power, sub–carrier centered NBI signals with $I_\mu = 1$, $1 \leq \mu \leq B$, $\kappa = 2$. Solid lines with markers: Simulated BER. Solid lines without markers: BER bound (8). Dashed lines: Asymptotic BER (19).
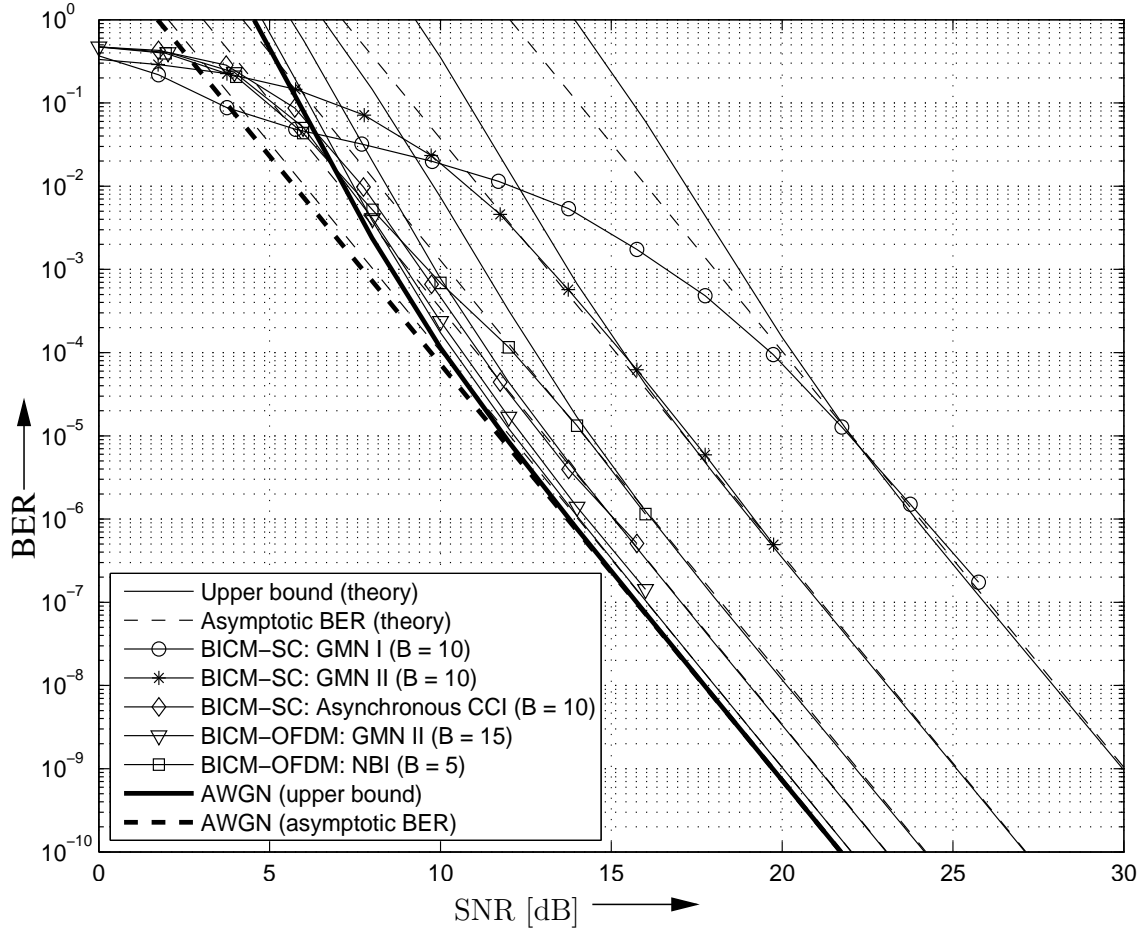
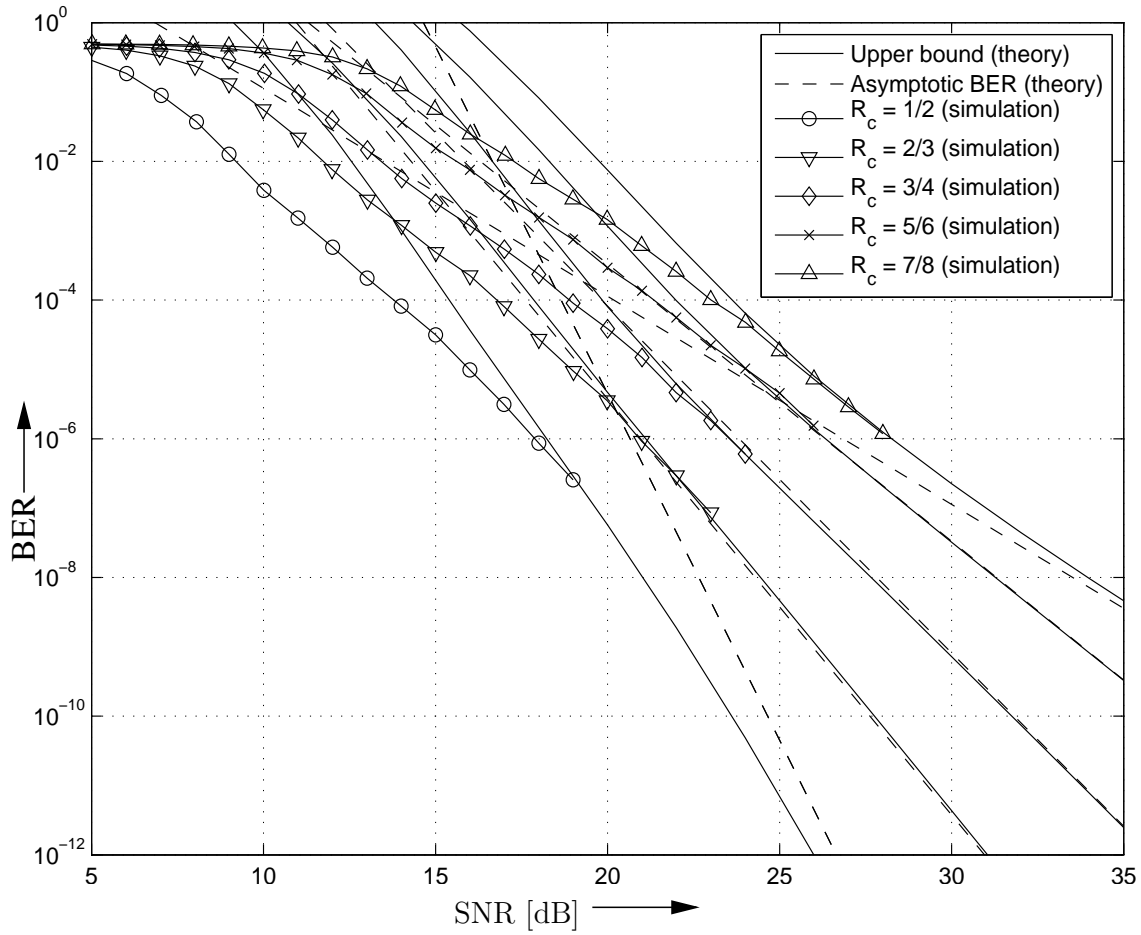Figure 2: BER of BICM–SC and BICM–OFDM impaired by various types of noise vs. SNR γ. Rayleigh fading, $R_c = 3/4$, 4–PSK, and $N_R = 1$. BICM–SC: $N = 972$ and $B_f T = 0.007$. BICM–OFDM: $N = 64$ and $L = 10$. GMN I: ϵ–mixture noise, $\epsilon = 0.01$, $\kappa = 100$. GMN II: ϵ–mixture noise, $\epsilon = 0.1$, $\kappa = 100$. Asynchronous CCI: Two asynchronous equal power 4–PSK CCI signals, $I_\mu = 1$, $\mu \in \{1, 2\}$, $I_\mu = 0$, $3 \leq \mu \leq 10$, raised cosine pulses $g_{1,\mu}(t)$, $\mu \in \{1, 2\}$, with roll–off factor 0.3, $\tau_{1,\mu} = 0.3T$, $\mu \in \{1, 2\}$, $\kappa = 2$. NBI: One sub–carrier–centered NBI signal, $I_1 = 1$, $I_2 = I_3 = I_4 = I_5 = 0$, $\kappa = 9$. Solid lines with markers: Simulated BER. Solid lines without markers: BER bound (8). Dashed lines: Asymptotic BER (19).

Figure 3: BER of BICM–OFDM impaired by NBI (3 equal power, sub–carrier–centered NBI signals, $I_1 = I_2 = I_3 = 1$, $\kappa = 10$) vs. SNR γ. I.i.d. Rayleigh fading, 64–QAM, $N = 128$, $B = 3$, and $N_R = 1$. Solid lines with markers: Simulated BER. Solid lines without markers: BER bound (8). Dashed lines: Asymptotic BER (19).
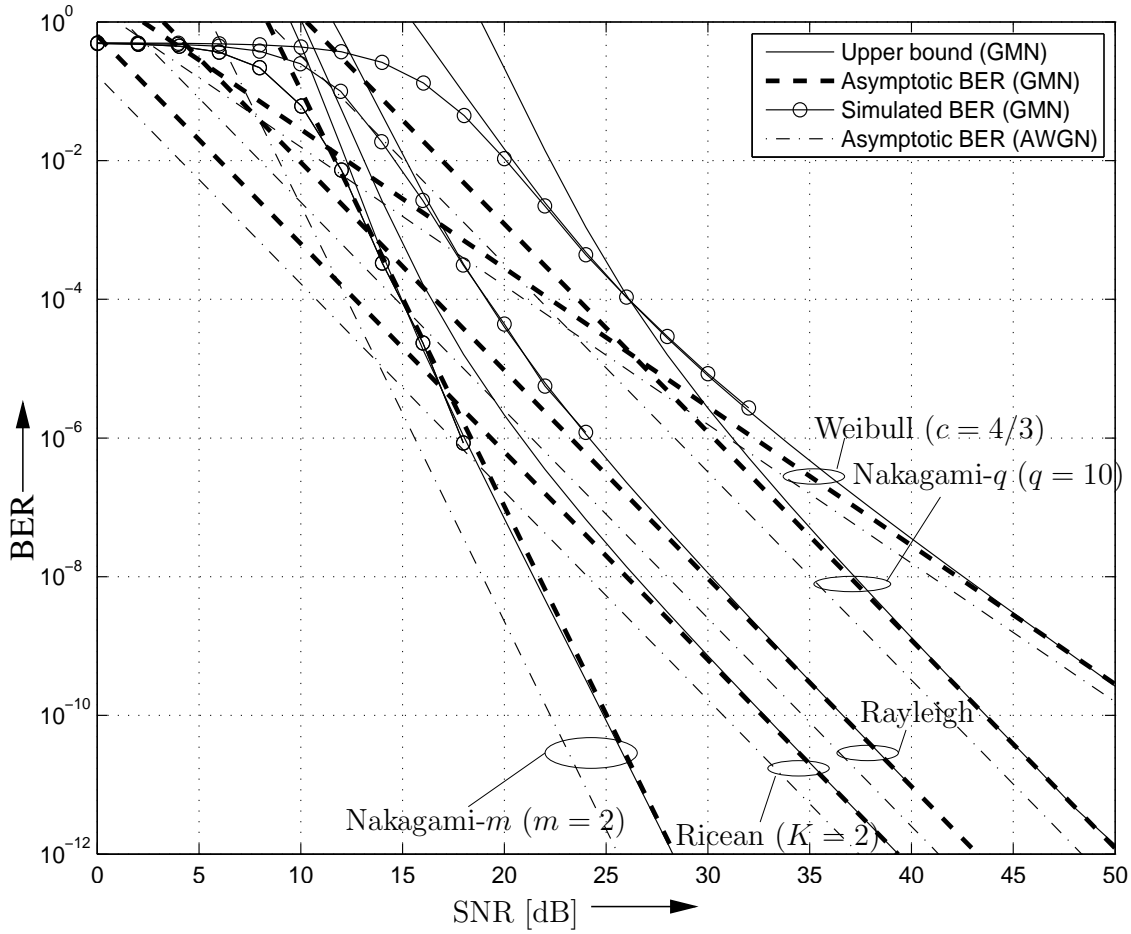
Figure 4: BER of BICM–SC impaired by GMN (ϵ–mixture noise, $\epsilon = 0.25$, $\kappa = 10$) and AWGN, respectively, vs. SNR γ. Ideal i.i.d. fading, $R_c = 7/8$, 16–QAM, and $N_R = 1$.
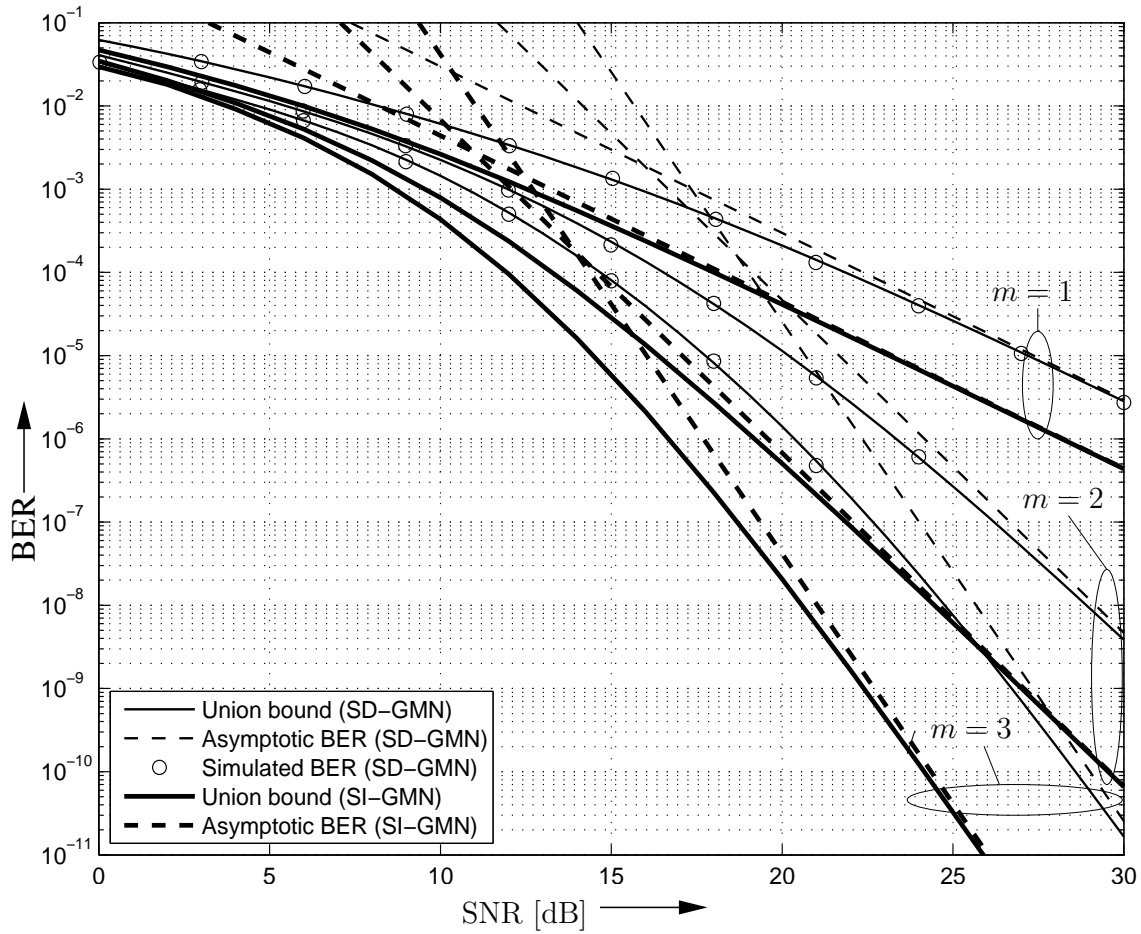
Figure 5: BER of uncoded SC transmission impaired by SD- and SI–GMN (ϵ–mixture noise, $\epsilon = 0.1$, $\kappa = 10$), respectively, vs. SNR γ. $N_R = 2$, Nakagami–m fading spatial correlation $\rho_a = 0.9$, and 4–PSK.
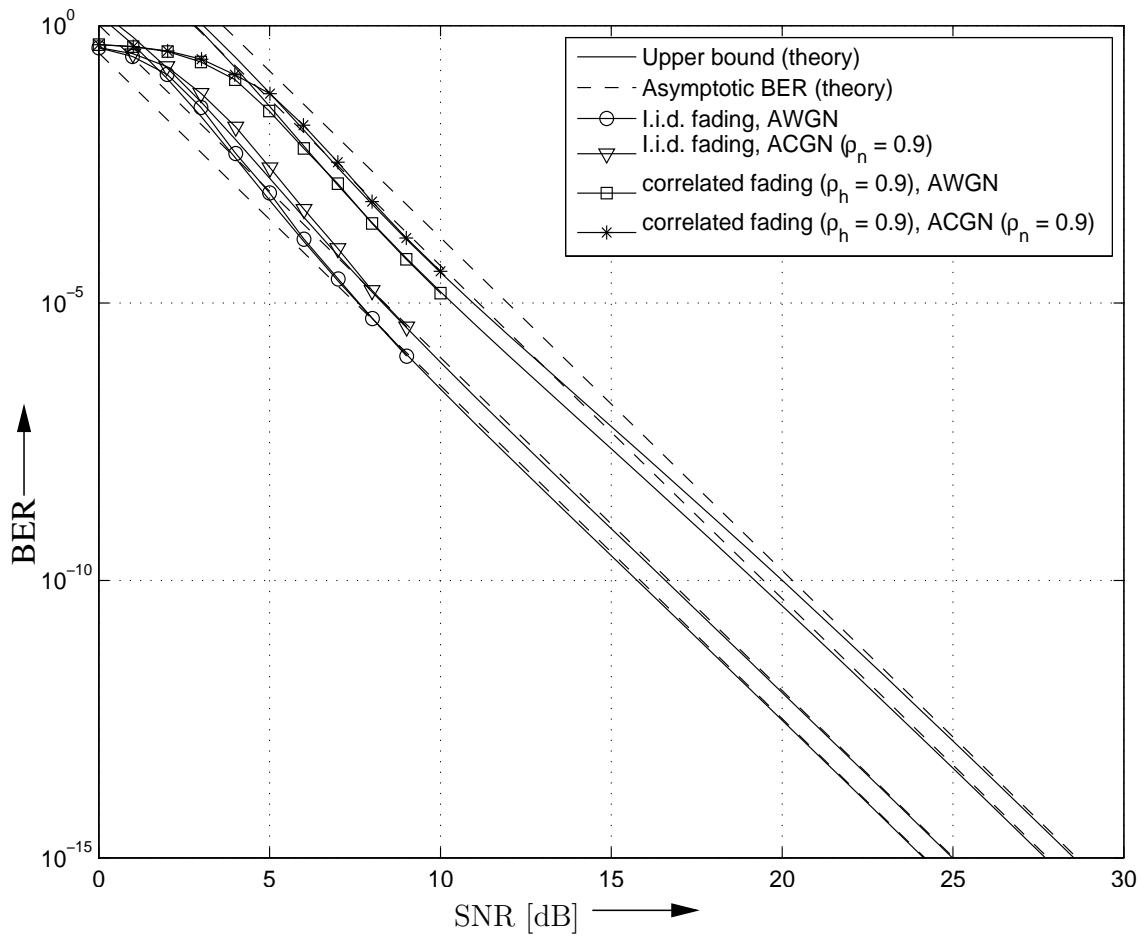
Figure 6: BER of BICM–SC impaired by AWGN/ACGN vs. SNR γ. Spatially i.i.d./spatially correlated, temporally i.i.d. Rayleigh fading, $R_c = 7/8$, 4–PSK, and $N_R = 2$. Solid lines with markers: Simulated BER. Solid lines without markers: BER bound (8). Dashed lines: Asymptotic BER (19).
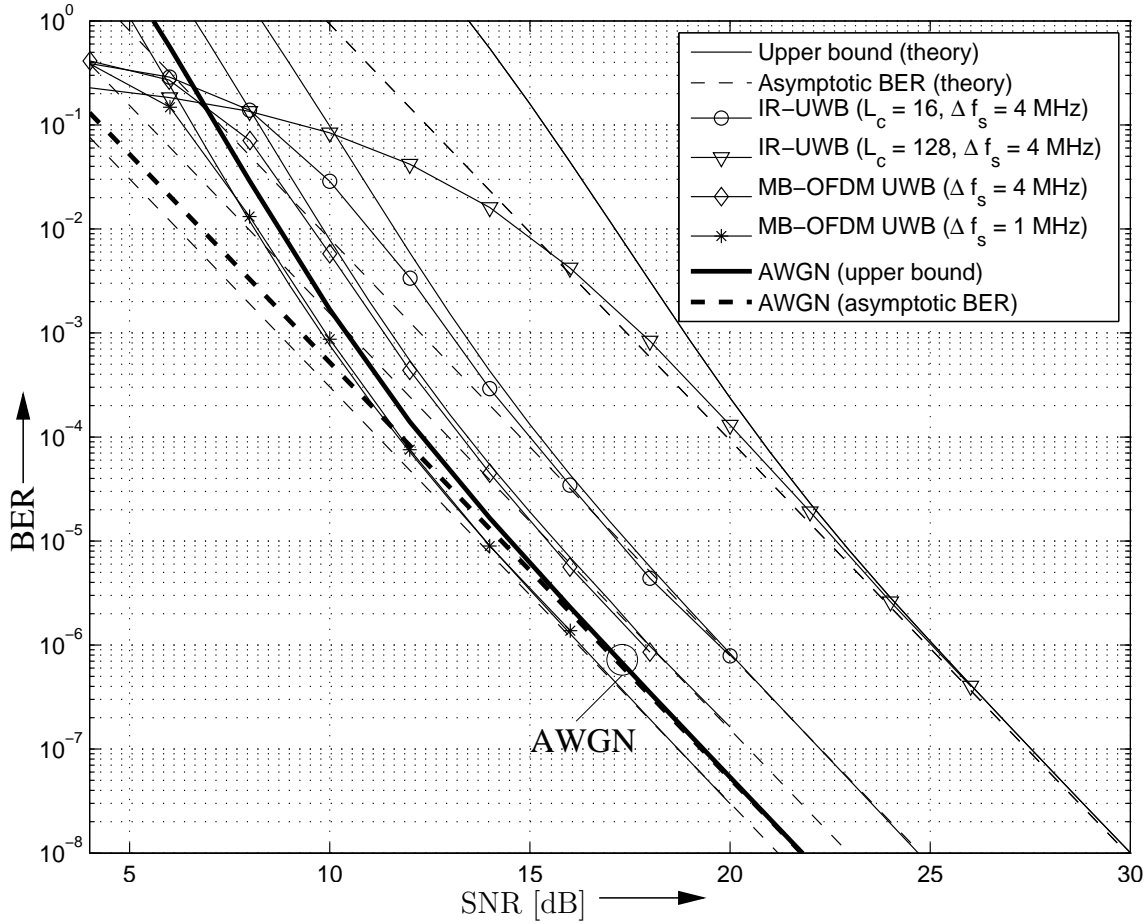
Figure 7: BER of BICM–OFDM system with sub–carrier spacing Δf_s impaired by IR–UWB [10] ($N_b = 8$ bursts per symbol and L_c chips per burst) and MB–OFDM UWB [9], respectively, vs. SNR γ. Ideal i.i.d. Rayleigh fading, $R_c = 5/6$, 4–PSK, and $N_R = 1$. Solid lines with markers: Simulated BER. Solid lines without markers: BER bound (8). Dashed lines: Asymptotic BER (19). For comparison the bound and the asymptotic BER for AWGN are also shown.